Thesis

presented by

Richard Slevin

in partial fulfilment of the requirements
for the Degree of Master of Science
in Agriculture and Environmental Sciences (ST2AE)
track: Global Forestry

Title

Ecohydrological Drivers and Limitation Transitions of Precipitation Induced Respiration in East African Savannas: Insights from a Hybrid Modelling Approach

Publicly defended on 14/November/2025

at AgroParisTech, France

in front of the following jury:

Prof. Dominique Serca	Examiner
Dr. Raphaël Manlay	Academic supervisor
Dr. Sonja Leitner	Host supervisor 1
Dr. Lutz Merbold	Host supervisor 2

ACKNOWLEDGEMENTS

I would like to express my deepest gratitude to my supervisors Dr. Lutz Merbold, Dr. Sonja Leitner, and Dr. Vincent Odongo for their invaluable guidance, constructive feedback, and continued encouragement throughout this project. Their expertise and patience have been fundamental in shaping both my scientific and personal approach to this thesis.

I gratefully acknowledge the support of the International Livestock Research Institute and Agroscope through the KADI Project, whose funding and institutional resources made this work possible.

I am sincerely thankful to Dr. Raphaël Manlay for his continued unwavering commitment and attention to my academic development throughout the GloFor programme.

Finally, I wish to thank my colleagues; Orla Kilroy, Emma Goddet, Giuseppe "Beps" Randon, Tosana Töben, Boris Llamas, Jannatul "Moon" Ferdous, Chetan Iragar, Taha Hashmi, Sachin Timilsina, Maria Adellia Widijanto, Matthew Tello Gonzalo, Juliette Bezy, Loïs Luijben, Lewin Weituschat, Pablo Canton, and Eamon O'Cathain.

I would not be the man I am today, without the adventures, festivities, lessons, and experiences I was so lucky to share with you all.

ABSTRACT

ENGLISH

Rainfall intensification is reshaping carbon-water dynamics in tropical drylands, yet the mechanisms governing respiration responses to rainfall pulses remain poorly quantified. This study investigates the ecophysiological drivers of Birch-pulses in an East African semi-arid savanna using the eddy-covariance technique between 2018–2020. High-frequency fluxes were segmented into rainfall-pulse sequences and analysed through empirical and data-driven modelling frameworks, including a moisture corrected method ($R_{moisture}$), an event segmented Peak–Tail (R_{PT}) model, and an explainable machine-learning model known as XGBoost.

The R_{PT} formulation reproduced respiration dynamics with higher accuracy (R^2 = 0.70; RMSE = 1.56 µmol m^{-2} s^{-1}) than temperature-only and $R_{moisture}$, successfully capturing short-term flux peaks and decay trajectories. SHAP-based feature importance revealed that hydrological rate and antecedent dryness metrics dominated variability, while temperature exerted a secondary, modulating influence. These results confirm that respiration pulses arise primarily from complex abrupt dry–wet transitions rather than rainfall magnitude or mean soil moisture.

Collectively, the findings advance the understanding of how antecedent hydrology, rewetting intensity, and thermal context interact to shape respiration in drylands. By integrating empirical and machine-learning approaches, this work provides a mechanistic framework for scaling and applying pulse-focused respiration partitioning to dryland sites across the region and beyond.

FRANÇAIS

L'intensification des précipitations modifie la dynamique carbone-eau dans les zones tropicales arides, mais les mécanismes régissant les réponses respiratoires aux impulsions pluviales restent mal quantifiés. Cette étude examine les facteurs écophysiologiques des impulsions pluviales dans une savane semi-aride d'Afrique de l'Est à l'aide de la technique de covariance des turbulences entre 2018 - 2020. Les flux à haute fréquence ont été segmentés en séquences d'impulsions pluviales et analysés à l'aide de cadres de modélisation empiriques et basés sur les données, notamment une méthode corrigée en fonction de l'humidité ($R_{moisture}$), un modèle Peak-Tail (R_{PT}) segmenté par événement et une approche XGBoost explicable.

La formulation R_{PT} a reproduit la dynamique de la respiration avec une plus grande précision (R^2 = 0,70 ; RMSE = 1,56 µmol m^{-2} s^{-1}) que la température seule et *Rmoisture*, capturant avec succès les pics de flux à court terme et les trajectoires de décroissance. L'importance des caractéristiques basée sur SHAP a révélé que le taux hydrologique et les mesures de sécheresse antérieure dominaient la variabilité, tandis que la température exerçait une influence secondaire et modulatrice. Ces résultats confirment que les impulsions respiratoires proviennent principalement de transitions complexes et abruptes entre la sécheresse et l'humidité plutôt que de l'ampleur des précipitations ou de l'humidité moyenne du sol.

Collectivement, ces résultats permettent de mieux comprendre comment l'hydrologie antérieure, l'intensité de la réhumidification et le contexte thermique interagissent pour façonner la respiration dans les zones arides. En intégrant des approches empiriques et d'apprentissage automatique, ces travaux fournissent un cadre mécanistique pour mettre à l'échelle et appliquer la partitionnement de la respiration axé sur les impulsions aux sites arides de la région et au-delà.

Table of Contents

1. INTRODUCTION

1.1. BACKGROUND

The productivity of East African drylands holds significance ranging from local- to international-scales. Intensifying rainfall regimes across the region are reshaping ecosystem functionality and the delivery of essential ecosystem services (Alan K. Knapp *et al.*, 2008). A comprehensive understanding of how these systems respond to shifting rainfall is therefore critical, not only for improving their representation in global greenhouse-gas inventories and climate models, and for guiding mitigation targets under the Paris Agreement, but also for informing context-specific adaptation and sustainable land-management strategies (Shukla *et al.*, 2019).

Across the region, food production, timber supply, climate regulation, water quality, and biodiversity are all being altered by shifting vegetation patterns, rising temperatures, and increasingly erratic precipitation (Anadón *et al.*, 2014) (Fig. 1). For smallholder farmers, rainfall irregularity disrupts planting calendars, reduces yields, and heightens food insecurity (Ndlovu *et al.*, 2020). Pastoralist households, often exceeding 100 head of cattle, face even sharper risks as forage and water availability fluctuate with erratic rainfall, causing greater mortality, reduced productivity, and mounting economic losses (Galvin, 2009). Extended droughts intensify competition over grazing lands and water, triggering land-tenure conflicts where communal rights overlap (Unks *et al.*, 2023 ; Galvin *et al.*, 2001). These trends threaten both the ecological integrity of landscapes and the livelihoods that depend on them, with subsistence communities being particularly exposed (Haile *et al.*, 2020 ; Senegal *et al.*, 2014).

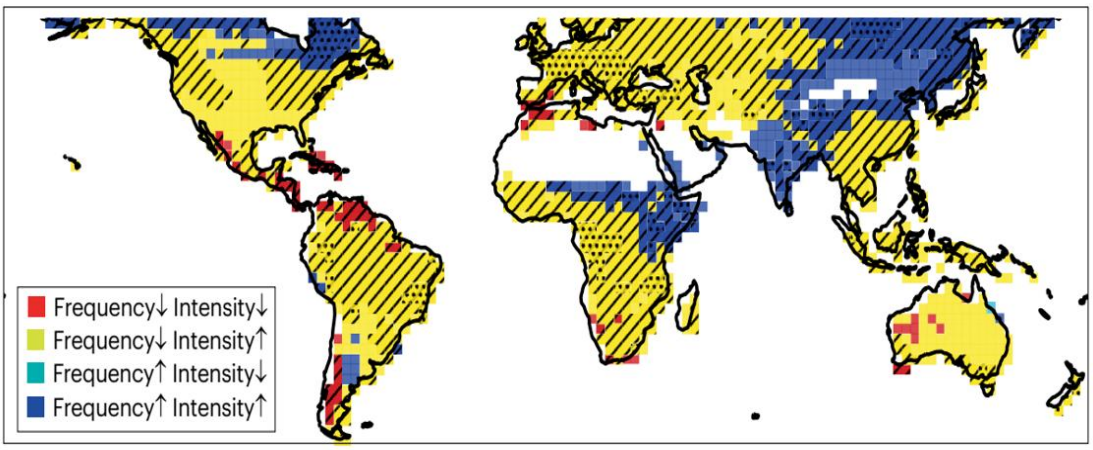

Figure 1: Covering ~41% of all land surface, CMIP6 projects more frequent and intense rainfall across tropical drylands, with pronounced effects in East Africa by 2050–2100. (Bastin; 2017, Feldman et al., 2024; Parracciani et al., 2023).

1.2. CLIMATIC AND ECOPHYSIOLOGICAL CONTEXT

Across much of the tropics, rainfall regimes are becoming increasingly uneven, with a rising share of annual precipitation delivered in fewer, higher-intensity events (Fischer *et al.*, 2013 ; Donat *et al.*, 2016 ; Douville *et al.*, 2021). Climate projections indicate that these trends will intensify under continued warming, producing longer dry intervals and heavier storms, especially in regions already prone to water limitation (Pendergrass et al., 2017;

Trenberth, 2011). With ecohydrological processes being governed less by total rainfall than by its temporal distribution, these hydrological shifts carry far-reaching consequences for dryland productivity (Jenerette *et al.*, 2008 ; Knapp *et al.*, 2008).

East Africa occupies a distinctive position within this global pattern. Unlike many subtropical regions projected to dry, it is expected to experience an overall increase in rainfall, although the spatial and seasonal distribution of these changes remains uncertain (IPCC, 2007). Regional rainfall is governed primarily by the seasonal migration of the Intertropical Convergence Zone (ITCZ), which produces a bimodal cycle with long rains from March to May and short rains from October to December (Nicholson, 2018). Superimposed on this cycle are major ocean–atmosphere modes, the Indian Ocean Dipole (IOD) and the El Niño–Southern Oscillation (ENSO), which influence rainfall timing and intensity as positive IOD and El Niño phases enhance moisture transport and flooding, while negative IOD and La Niña phases suppress convection and extend droughts in the region (Abram *et al.*, 2008 ; Palmer *et al.*, 2023). Under climate change, extreme IOD and ENSO events are projected to become more frequent and intense, amplifying this variability that defines the region's hydroclimate (Cai et al., 2014; Wang et al., 2024).

This climatic variability occurs within an ecological context dominated by arid, semi-arid, and dry sub-humid zones across Kenya, Ethiopia, and northern Tanzania, sustaining the open savannas and grasslands that shape the region's ecological identity (Haile *et al.*, 2020 ; Niang *et al.*, 2017). These ecosystems are fundamentally water-limited, with productivity, nutrient cycling, and microbial activity driven by the sporadic arrival of rainfall rather than gradual seasonal progression (Schwinning & Sala, 2004 ; Huxman *et al.*, 2004). Warm temperatures and high potential evapotranspiration intensify this constraint, ensuring that even brief dry intervals rapidly deplete available soil moisture (Kew *et al.*, 2021). When rainfall does occur, its distribution between infiltration and runoff dictates whether water recharges the root zone or is lost from the system (Alan K Knapp *et al.*, 2008).

Dryland ecology has adapted to this oscillating pattern of stress and release, as woody and herbaceous species exhibit deep or dimorphic rooting strategies, high water-use efficiency, and the capacity for rapid photosynthetic activation following rewetting (Seghieri, 1995 ; Lindh *et al.*, 2014). Soil microbial communities likewise tolerate desiccation and resuscitate quickly when moisture returns, driving short bursts of metabolic activity (Collins *et al.*, 2008). These adaptations enable persistence under scarcity but also make biological processes highly sensitive to the timing and intensity of individual rain events.

1.3. THE BIRCH EFFECT

A key manifestation of dryland climatic sensitivity is the Birch effect; an ephemeral, multi-phase rise in Ecosystem Respiration (Reco) following rewetting after an extended dry period (Birch, 1958) (Fig. 2). This short-lived respiratory surge results from the sequential interplay of physical gas displacement, microbial resuscitation, and plant physiological responses, each acting on distinct timescales (Placella *et al.*, 2012 ; Schimel, 2018). The effect is reported across a variety of sub-Saharan and global sub-tropical ecosystems, attesting to its ubiquity and global biogeochemical significance (Ago *et al.*, 2016 ; Wieckowski *et al.*, 2024 ; Metz *et al.*, 2023 ; Vardag *et al.*, 2025). Across these environments, Birch-pulses are often treated as an anomaly, yet evidence shows that they disproportionately contribute ~12–25% of Reco in highly intermittent precipitation

regimes (Manzoni *et al.*, 2020 ; Nguyen *et al.*, 2025 ; Huxman *et al.*, 2004 ; Emmerich, 2003).

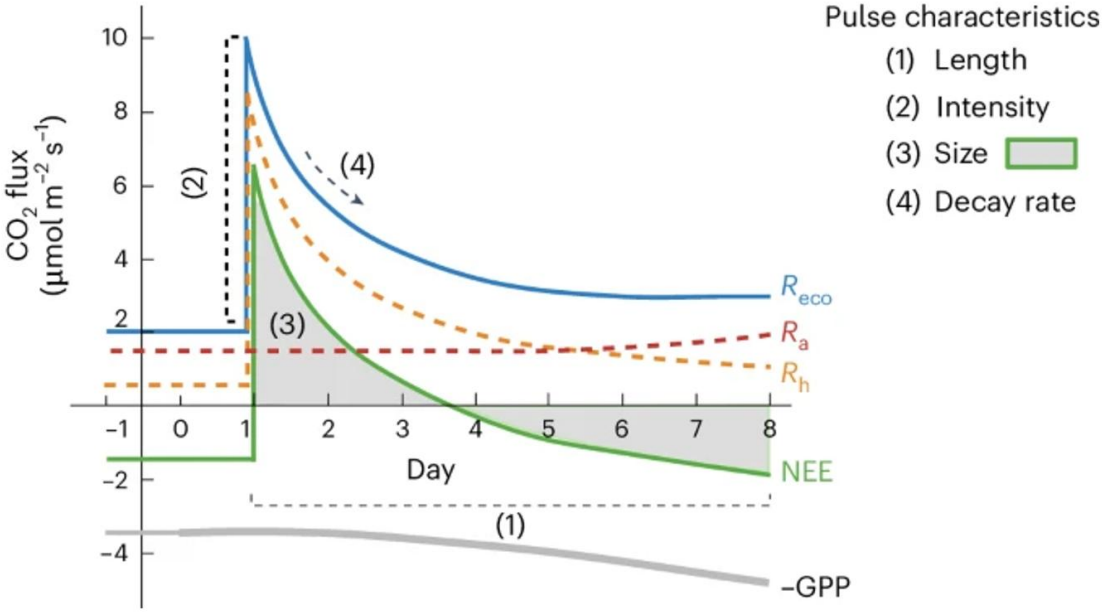

Figure 2: Conceptual representation of the Birch effect showing post-rewetting flux dynamics with key magnitude characteristics denoted. Adapted from Nguyen et al. (2025).

CO_2 Displacement

The initial phase of the Birch response is largely abiotic. During prolonged drought, subsurface CO_2 accumulates in soil pores as limited autotrophic and heterotrophic respiration persist under restricted diffusion (Frouz & Bujalský, 2018). When rainfall infiltrates, the advancing wetting front produces a displacement effect that physically expels this stored gas, generating an abrupt CO_2 flush (Singh *et al.*, 2023 ; Huxman *et al.*, 2004 ; Sánchez-García *et al.*, 2020). The magnitude of this efflux depends on the soil's physical structure; bulk density, texture, organic-matter content, and macropore connectivity, all regulating infiltration efficiency and expulsion capacity (Beven & Germann, 1982 ; Jarvis *et al.*, 2007). In fine-textured vertisols common to East African savannas, repeated shrink–swell cycles continually alter pore networks and gas transport (Schimel *et al.*, 2007). Overall, the intensity of this phase of the pulse scales with the duration and severity of antecedent drought, which control pore desiccation and CO_2 storage prior to rainfall (Singh *et al.*, 2023).

Microbial Dynamics under Dry–Wet Cycles

After the initial displacement phase, interpore soil-water films reconnect and the diffusion of substrates and oxygen improves, rapidly restoring microbial metabolism (Schimel, 2018). These microbial communities exhibit strong physiological regulation to survive desiccation by adopting osmoregulatory mechanisms to maintain internal water potential during anhydrous conditions (Warren, 2014 ; Schimel *et al.*, 2007).

Upon rapid rewetting, osmotic stress reverses abruptly, cell membranes rupture releasing osmolytes and labile organic compounds into the environment that provide immediate substrates for respiration (Kieft *et al.*, 1987 ; Lado-Monserrat *et al.*, 2014 ; Warren, 2014 ; Wood *et al.*, 2001). Metabolic activity rebounds within hours, producing a transient surge in CO_2 efflux as a result of this mineralisation of microbial necromass that was accumulated under drought stress (Manzoni *et al.*, 2020 ; Schimel *et al.*, 2007).

A variety of physico–temporal feedbacks amplify this response, as repeated drying–rewetting cycles disrupt soil aggregates, enhance oxygen diffusion, and expose formerly protected organic matter to decomposition (Rabbi *et al.*, 2024). Pulse magnitude naturally scales with drought severity and duration, as extended dry periods promote greater substrate accumulation and intensify hypo-osmotic stress upon rewetting, producing stronger and more sustained CO_2 releases (Singh *et al.*, 2023 ; Manzoni *et al.*, 2012).

LAGGED PLANT FACILITATED READJUSTMENT

As labile carbon pools are depleted, post-rainfall Reco declines within hours to days, sustaining productivity through a subsequent dry-down phase (Canarini *et al.*, 2019 ; Placella *et al.*, 2012). As leaf rehydration, stomatal reopening, and enzymatic reactivation resolve over several days, Gross Primary Productivity (GPP) eventually re-establishes equilibrium as photosynthesis recovers and intensive microbial resource competition subsides, marking the end of the transient carbon imbalance (Chen *et al.*, 2009 ; Sala & Lauenroth, 1982 ; Jiang *et al.*, 2021).

1.4. RESEARCH RATIONALE

MECHANISTIC UNCERTAINTIES IN RAINFALL-INDUCED RECO

While rainfall pulses are recognized as dominant drivers of biogeochemical fluxes in drylands, the mechanistic basis of their variability remains insufficiently understood (Liang *et al.*, 2023). Most existing frameworks describe Birch-pulses as uniform, short-lived CO_2 flushes, overlooking how the complex interaction of temporal, thermal, and moisture contexts shape their timing and magnitude. Consequently, our understanding of how pulse responses differ across climatic and edaphic contexts is still fragmentary. Understanding these process-level dynamics is critical for predicting ecosystem carbon balance and resilience under intensifying rainfall variability, particularly in regions that sustain major food production and pastoral systems (Barnes *et al.*, 2021).

GEOGRAPHIC ASYMMETRIES IN FLUX OBSERVATIONS

Given the technocratic and capital-intensive nature of Eddy-Covariance (EC) systems, infrastructure has concentrated global flux research within well-funded institutions of the Global North (Stoy *et al.*, 2023). As a result, coverage is spatially skewed toward temperate ecosystems, while tropical and subtropical regions, home to many developing countries and some of the world's most climate-sensitive biomes, remain under-represented. Historically, Africa has contained only 3.7 % of global flux measurement sites, revealing a persistent spatial bias that limits empirical representation of the continent's climate-sensitive ecosystems (Burba, 2019). This gap is particularly acute for savanna ecosystems,

which dominate vast tracts of the sub-Saharan landscape yet remain among the least instrumented biomes globally. This geographic asymmetry embeds systemic bias in the empirical foundations of biogeochemistry, undermining the representativeness of the models built to tackle the borderless problem of climate change (Bieri *et al.*, 2022). The result is a feedback loop in which data scarcity perpetuates underrepresentation, constraining both the scientific understanding and policy relevance of dryland ecosystems in global climate affairs. Expanding knowledge of tropical dryland systems is therefore vital to sustaining resilience under intensifying climatic instability (Jung *et al.*, 2009).

MODEL LIMITATIONS IN REPRESENTING PULSE DYNAMICS

Prevailing ecosystem models capture broad seasonal patterns but fail to reproduce the abrupt event-scale, non-linear dynamics that define dryland fluxes (Barnes *et al.*, 2021). Standard formulations rely on temperature-response functions that neglect the strong and variable moisture dependencies characteristic of drylands (Reichstein *et al.*, 2005 ; Wang *et al.*, 2014). Even the recently developed FluxPulse model (Nguyen *et al.*, 2025), while introducing an event-scale correction, remains largely geometric, emphasizing form rather than the underlying ecophysiological mechanisms governing post-rain responses. Current models cannot capture the abrupt transitions between dry and wet states, whereas purely empirical fits offer limited explanatory insight into why pulse intensity varies (Meyer *et al.*, 2018).

A new modelling approach is therefore required that integrates mechanistic interpretability with empirical accuracy, bridging the divide between statistical fitting and ecophysiological understanding (Ai *et al.*, 2023). By embedding event-scale process representation within a statistical framework, this study aims to advance both the realism and the explanatory power of modelling Reco in water-limited ecosystems (Dannenberg *et al.*, 2023).

1.5. RESEARCH QUESTION

What are the ecophysiological drivers of Birch-pulses, and how do they regulate Ecosystem Respiration in an East African dryland savanna?

1.6. HYPOTHESES

- H1: Birch-pulse event magnitude is primarily governed by antecedent soil moisture characteristics, with temperature exerting a secondary effect.
- H2: Integrating event segmentation and soil-moisture context improves the accuracy and representation of Reco variability compared to temperature-only formulations.
- H3: Non-linear interactions among hydrological, thermal, and temporal covariates explain the complex transition from water- to temperature-limited Reco.

2. MATERIALS AND METHODS

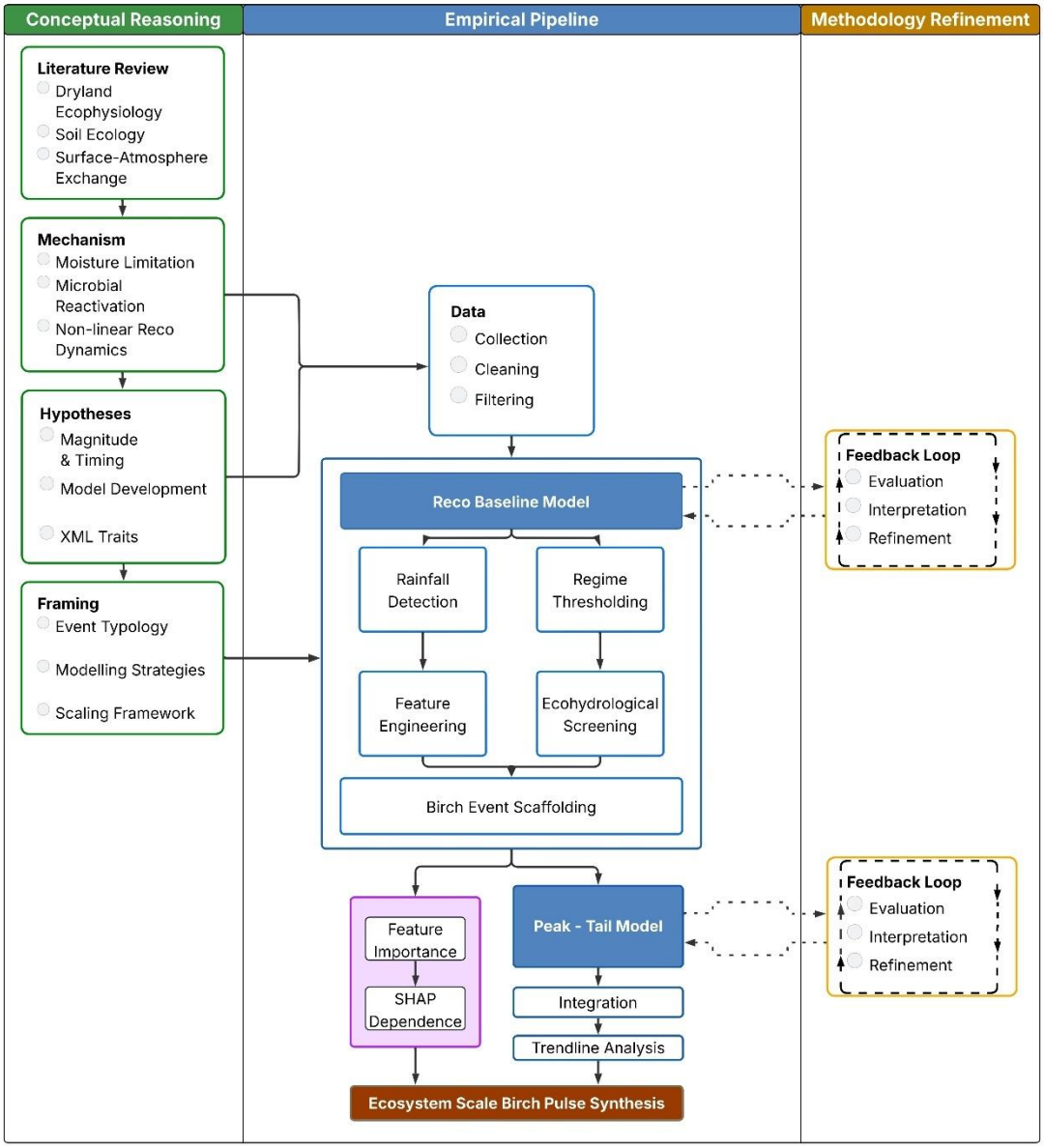

Figure 3: Conceptual framework illustrating the a priori structure and rationale of the study, linking ecophysiological theory with empirical modelling to guide the detection, analysis, and synthesis of Birch-pulse dynamics across scales.

2.1. STUDY SITE

The study was conducted at the ILRI Kapiti Research Station, a 128 km² semi-arid savanna in Machakos County, Kenya (Odongo *et al.*, 2025). Mean annual rainfall is ≈ 550 mm yr^{-1}, distributed bimodally with wet seasons in March–May and October–December (Fig. 4).

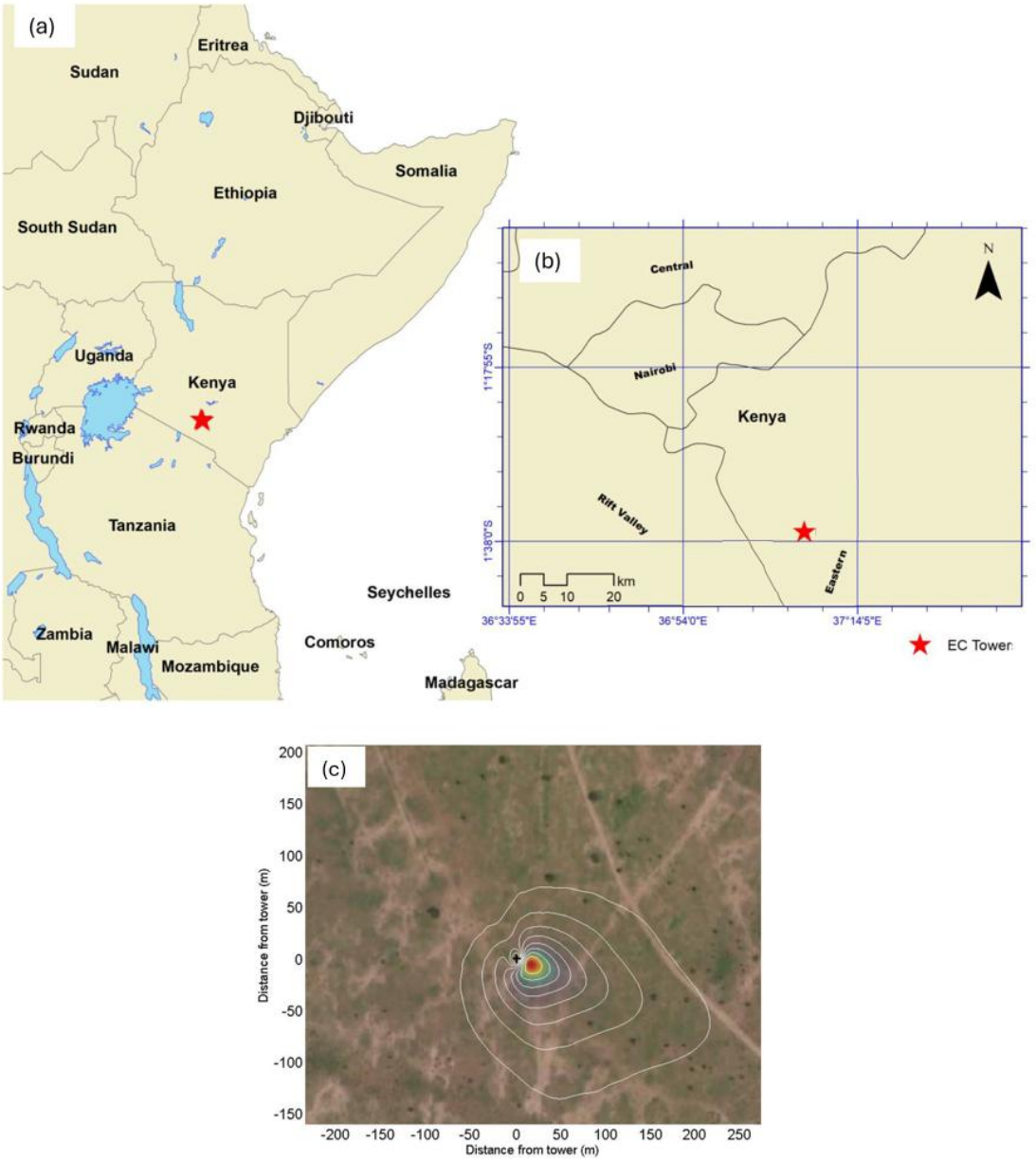

Figure 4: (a) Regional context of the site. (b) Position of EC tower within south central Kenya. (c) High-resolution footprint climatology overlaid on satellite imagery showing the dominant flux contribution areas surrounding the tower (Odongo *et al.*, 2025).

Vegetation is dominated by a mix of perennial C_3 and C_4 grasses; *Cynodon dactylon* (L.) Pers., *Setaria trinervia* (Schumach.) Stapf, *Themeda triandra* Forssk., *Microchloa kunthii* Desv., and *Digitaria macroblephara* Hack., interspersed by forbs and sparse woody cover such as *Vachellia nubica* (Benth.) Kyal. & Boatwr (Muthoka *et al.*, 2025). Soils comprise a Vertisol–Cambisol mosaic controlling local hydrology and vegetation dynamics. Measurements were collected at the Kapiti Flux Tower (1.63° S, 37.19° E;1731m a.s.l.) (Fig. 5).

Figure 5: Kapiti, a semi-arid savanna, with the EC tower situated above the study area. The landscape comprises open savanna with scattered shrubs and occasional *Vachellia* shrubs (Photo: L Merbold).

2.2. Data Acquisition

Eddy Covariance Theory and Operation

The EC method quantifies turbulent exchange of gases, heat, and momentum between the land surface and atmosphere (Aubinet *et al.*, 2012). Instantaneous flux density is defined as:

$$F_c = \overline{w'c'}$$

where:

- F_c is the vertical turbulent flux of CO_2 (μmol CO_2 m^{-2} s^{-1}),
- w' is the instantaneous deviation of vertical wind velocity from its mean (m s^{-1}),
- c' is the instantaneous deviation of CO_2 concentration from its mean (μmol mol^{-1}), and
- $\overline{w'c'}$ denotes the time-averaged covariance between vertical velocity and CO_2 concentration fluctuations.

Positive F_c indicates upward fluxes; negative values denote ecosystem uptake. Sampling at 10 Hz resolves the dominant turbulence frequencies driving vertical transport across the footprint yielding continuous, non-destructive measurements of ecosystem-atmosphere exchange (Fig. 6, 7).

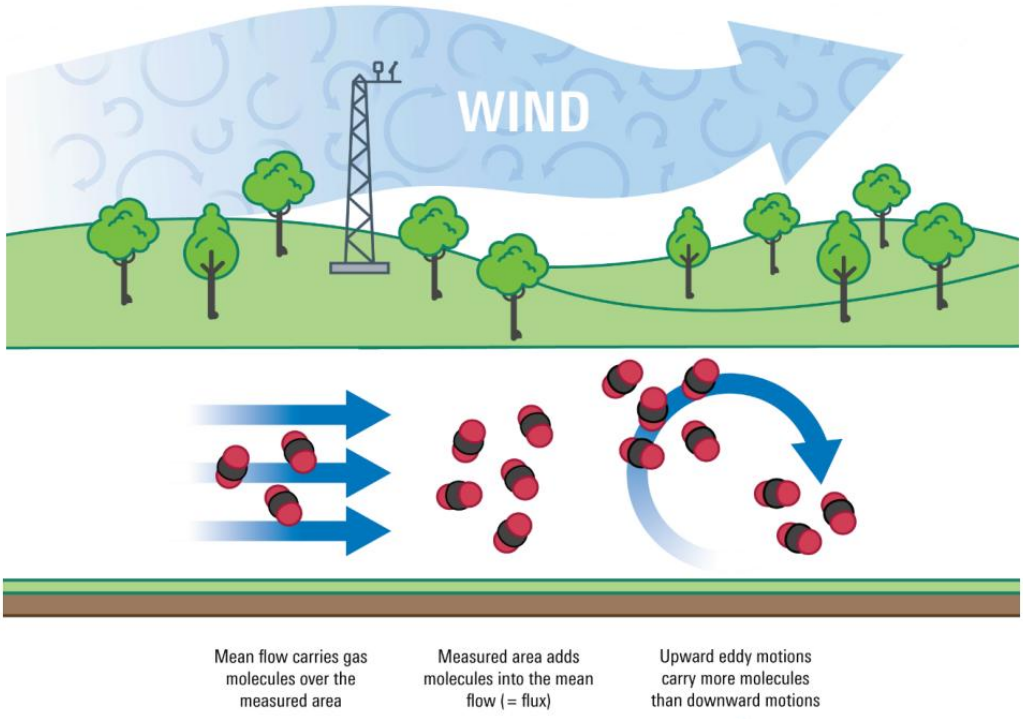

Figure 6: Conceptual illustration of the EC principle. Vertical wind fluctuations transport gas molecules between the surface and atmosphere: a flux arises when turbulent eddies create a net upward or downward transfer of gases (SCF, 2025).

EDDY COVARIANCE INSTRUMENTATION

Wind components and sonic temperature were measured using a 3D sonic anemometer, which derives vertical and horizontal wind vectors from ultrasonic pulse travel times along three non-coplanar paths (Kaimal & Finnigan, 1994). The instrument was mounted at 4.3 m and oriented north toward the prevailing wind to minimise flow distortion.

An open-path infrared gas analyser (IRGA) was co-located within the anemometer's sampling volume (5cm N, 20cm E) to ensure both instruments sampled the same air parcel, reducing phase lag and covariance loss (Burba *et al.*, 2008). The IRGA measured CO_2 and H_2O densities via differential absorption of two infrared wavelengths. Instantaneous gas concentrations were synchronised with wind data to compute covariances in real time.

The open-path design provided high temporal resolution and avoided tubing attenuation. Optical windows were cleaned weekly, and calibration with certified CO_2 standards was performed biannually. Regular alignment checks and inspection for contamination or temperature drift ensured instrument stability and geometric accuracy. The full suite of sensors (Fig. 7), their configuration, and specifications is provided in Appendix 1, Table A1, and processing workflow in Appendix 2.

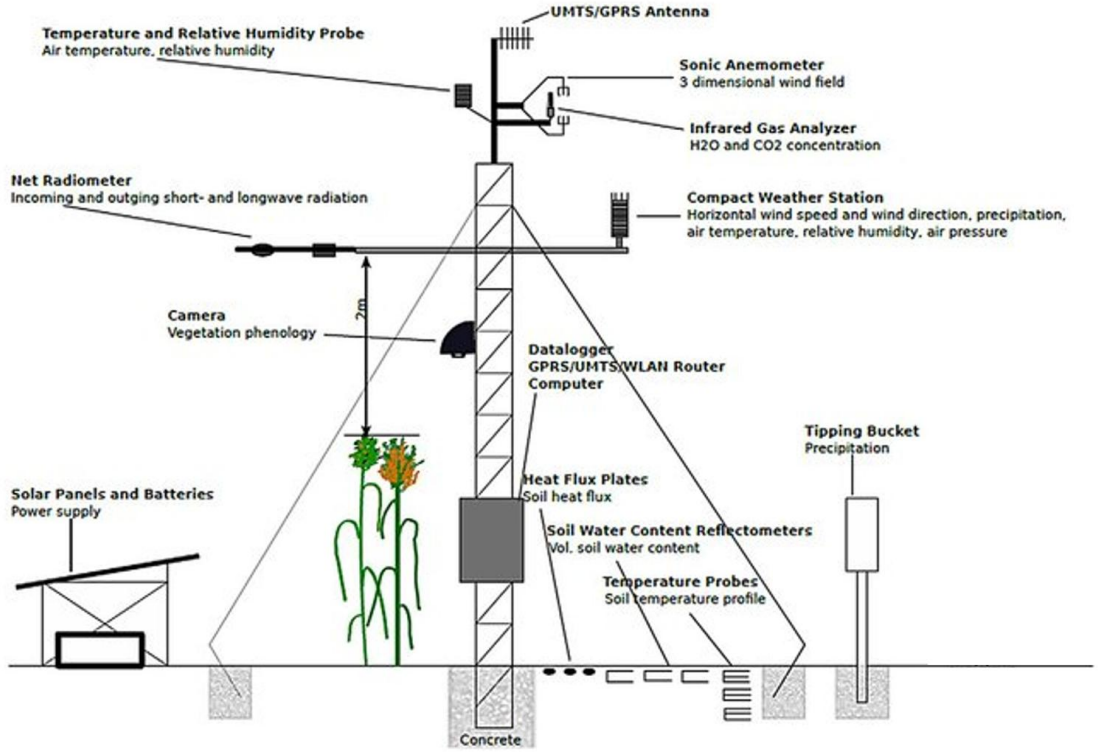

Figure 7: Schematic layout of a typical EC tower setup, illustrating the suite of core flux instruments alongside the biometeorological sensors (Bliefernicht *et al.*, 2018).

2.3. DATA ANALYSIS

RAIN-PULSE DETECTION

To isolate hydrologically meaningful rainfall events, precipitation was aggregated using a 6-hour rolling window. A wet onset was defined when cumulative rainfall within any 6-hour interval reached ≥5mm. The wet offset was identified as the first subsequent 6-hour interval with zero rainfall. All contiguous intervals meeting these criteria were grouped as a wet sequence.

To ensure temporal alignment with 30-min EC and soil-moisture data, each wet sequence was re-projected onto the native 30-min timestep. Two adjustments were applied:

1. Retroactive onset refinement: tracing backward from the first 30-min step within the 6-h wet window to the earliest non-zero rainfall, defining the true wet onset.
2. Forward offset refinement: extending the wet period to the last 30-min step with measurable rainfall before a continuous dry interval began.

Each complete dry-wet transition was assigned a unique ID, establishing the structural framework for subsequent event-scale covariate computation (Fig. 8).

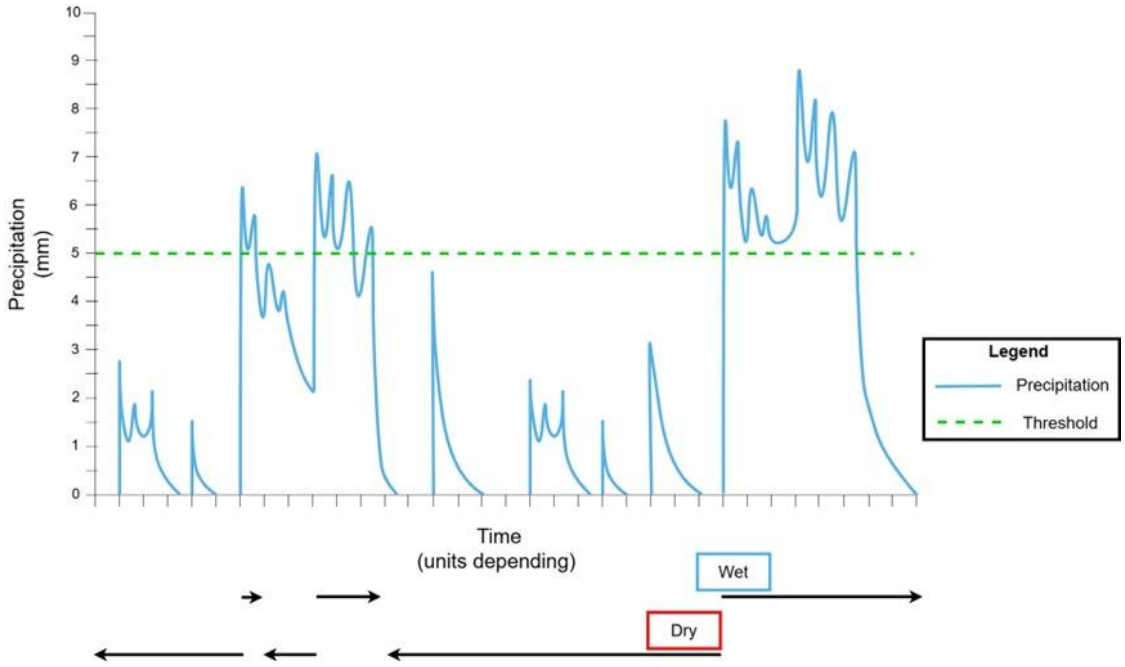

Figure 8: Conceptual illustration of rainfall thresholding and event classification. Periods exceeding the defined precipitation threshold (green dashed line) are identified as *wet*, while intervening intervals are classified as *dry*.

ENVIRONMENTAL COVARIATES

To characterise the ecohydrological conditions associated with each rainfall pulse, a set of environmental covariates was derived at 30-min resolution and is detailed in Appendix 2, Table A2.

Soil-moisture normalisation indices standardised site-specific metrics into ecologically relevant fractions, removing depth and texture effects, while differential and cumulative metrics represented short-term rewetting, and antecedent desiccation. Hydrological balance metrics described total and cumulative precipitation and evapotranspiration, antecedent water deficits, and running climatic stress, linking rainfall inputs to surface water balance. Temporal descriptors expressed the relative position of each observation within the wet–dry sequence, distinguishing early, peak, and late pulse conditions.

RECO MODEL DEVELOPMENT

To identify the transition between water- and temperature-limited regimes, a Non-Rectangular Hyperbola (NRH) was fitted to Reco as a function of Relative Soil Water Content (RSWC).

A model was developed to represent steady-state, non-pulse period Reco, following the standard temperature-response formulation of Reichstein et al. (2005) and extended via a generalised additive model (GAM) to incorporate non-linear soil-moisture and temperature–moisture interactions:

$R_{moisture} =$

$$\beta 0 + s(T_{sh}) + s(T_{mid}) + s(SWC_{sh}) + s(SWC_{mid}) + ti(T_{sh}, SWC_{sh}) + ti(T_{mid}, SWC_{mid}) + \varepsilon$$

where:

- $R_{moisture}$: predicted nighttime Reco (μmol CO_2 m^{-2} s^{-1}),
- β_0 : model intercept,
- T_{sh} & T_{mid} : shallow and mid-depth soil temperatures (°C),
- SWC_{sh} & SWC_{mid} : shallow and mid-depth soil water contents (m^3 m^{-3}),
- $s()$: smooth spline functions,
- $ti()$: tensor-product interaction smooths between temperature and soil moisture,
- ε : model residual error term.

The model, fitted to nighttime data (PPFD < 10 μmol m^{-2} s^{-1}) outside potential pulse periods, isolates Reco by selecting all positive (Net Ecosystem Exchange) NEE values within this low-light range, representing conditions where photosynthetic uptake is negligible and gross primary productivity (GPP) is assumed to be zero, so NEE ≈ Reco (Reichstein, 2005). This approach captures respiration variability across both thermal and hydrological gradients while minimizing dry-season bias.

Residuals were defined as

$$\varepsilon_t = R_{\text{obs},t} - R_{\text{pred},t}$$

Significant positive deviations were identified using a one-sided Upper Prediction Interval (UPI):

$$UPI_t = R_{\text{pred},t} + k\sigma_t$$

where σ_t is model error and *k=2* approximates the 97.5th percentile under Gaussian residuals. Timesteps within wet sequences where $R_{\text{obs},t} > UPI_t$were flagged as anomalies; fluxes exceeding expected temperature–moisture responses.

PEAK-TAIL SEGMENTATION

Within each wet window, anomalous timesteps were clustered into events based on continuity.

- Peak: $R_{\text{obs},t} > UPI_t$
- Tail: $R_{\text{moisture},t} < R_{\text{obs},t} \leq UPI_t$

The first exceedance above the UPI marked the Birch onset, and the last tail value above baseline marked the Birch termination, classifying the timeframe of each birch event. R_{moisture} was applied across Peak and Tail phases and merged with non-pulse predictions to produce a continuous estimate capturing Birch-pulse deviations within the full time series.

MODEL CALIBRATION AND EVALUATION

Nighttime Reco was used to train three formulations:

1) R_{temp}: Temperature-response exponential baseline (Reichstein *et al.*, 2005),
2) $R_{moisture}$: Moisture-corrected GAM, and
3) R_{PT}: Model explicitly trained on transient Peak–Tail phases.

MODEL PERFORMANCE EVALUATION

Model performance was quantified by:

$$R^2 = 1 - \frac{\sum(R_{\text{obs}} - R_{\text{pred}})^2}{\sum(R_{\text{obs}} - \bar{R_{\text{obs}}})^2}$$

$$RMSE = \sqrt{\frac{1}{n}\sum(R_{\text{obs}} - R_{\text{pred}})^2}$$

$$MAE = \frac{1}{n}\sum \mid R_{\text{obs}} - R_{\text{pred}} \mid$$

$$Bias = \frac{1}{n}\sum(R_{\text{pred}} - R_{\text{obs}})$$

and scale-independent diagnostics:

Nash–Sutcliffe Efficiency (NSE): = R^2 relative to mean observations.

Capture Ratio:

$$\sum R_{\text{pred}} / \sum R_{\text{obs}}$$

EVENT-LEVEL CARBON INTEGRATION

Reco during each Birch event was integrated from 30-min fluxes converted from μmol CO_2 m^{-2} s^{-1} to g C m^{-2} (12×10^{-6} g C μmol^{-1} CO_2) using the trapezoidal rule:

$$C_{\text{event}} = \sum_i \frac{(R_{pred} + R_{pred+1})}{2} \Delta t_i, \Delta t_i = 1800s$$

Integrations were applied to observed and modelled fluxes to derive total event carbon release, bias, and cumulative model differences. Event integrals supported aggregation and distribution analyses.

DYNAMIC TRAJECTORY AND SHAPE METRICS

To evaluate how well models reproduced event-scale temporal patterns, shape-comparison metrics were applied to the modelled flux trajectories. Dynamic Time Warping (DTW) quantified the temporal alignment cost between observed and modelled fluxes.

$$DTW(R_{obs}, R_{pred}) = \frac{min}{\pi} \sum_{(i,j)\varepsilon\pi} w_i |R_{obs,i} - R_{pred,j}|$$

where:

- π : optimal warping path aligning indices i and j,
- w_i : weighting factor that increases near the event peak to emphasize timing fidelity.

Lower DTW values indicate closer temporal agreement between the observed and modelled flux dynamics.

Spearman's rank correlation coefficient (ϱ) measured monotonic associations between ranked variables:

$$\frac{cov(r_x, r_y)}{\sigma_{r_x}\sigma_{r_y}}$$

where:

- *cov* : covariance between the ranked variables,
- r_x & r_y : rank-transformed values of x and y

Cosine similarity measured geometric similarity independent of magnitude:

$$\frac{\sum(R_{\text{obs}} \cdot R_{\text{pred}})}{\| R_{\text{obs}} \| \| R_{\text{pred}} \|}$$

A weighted NSE was computed on duration- and amplitude-normalized trajectories, giving greater weight to high-magnitude phases and isolating structural rather than absolute discrepancies.

EXPLAINABLE MACHINE-LEARNING ANALYSIS

An Explainable Machine Learning (XML) gradient-boosted decision-tree model (XGBoost) quantified the influence of ecohydrological, and climatic covariates defined in Section 2.3.3 (Chen & Guestrin, 2016).The model was trained on 70%, validated on 10 %, and tested on 20% of Birch-pulse data (Friedman, 2009 ; Goodfellow, 2016).

Hyperparameters were optimized through five-fold cross-validation to minimize out-of-sample RMSE (James *et al.*, 2013). Feature contributions were interpreted using Shapley Additive Explanations (SHAP), which decompose predictions into additive feature effects while preserving local accuracy (Lundberg *et al.*, 2020). SHAP values quantify both the magnitude and direction of each variable's influence on the model output, indicating how much each covariate increases or decreases Reco for every observation. Mean absolute SHAP values provided global importance rankings, while dependence plots derived from the independent test dataset revealed how these effects evolved across the range of each predictor, highlighting thresholds and interactions when coloured by secondary features (Rudin, 2019). Together, combined with the model's high predictive accuracy, enabled inference of real-world ecohydrological interactions, revealing how covariates jointly regulated Reco.

3. RESULTS

3.1. RECO MOISTURE CONTROLS AND CONSTRAINTS

Reco exhibited a non-linear response to soil moisture (Fig. 9). A Non-Rectangular Hyperbola fitted to Reco as a function of RSWC revealed a hyperbolic response with an inflection at RSWC ≈ 0.348, separating moisture- and temperature-limited regimes, with efflux rising sharply under dry conditions and approaching an asymptote at higher moisture.

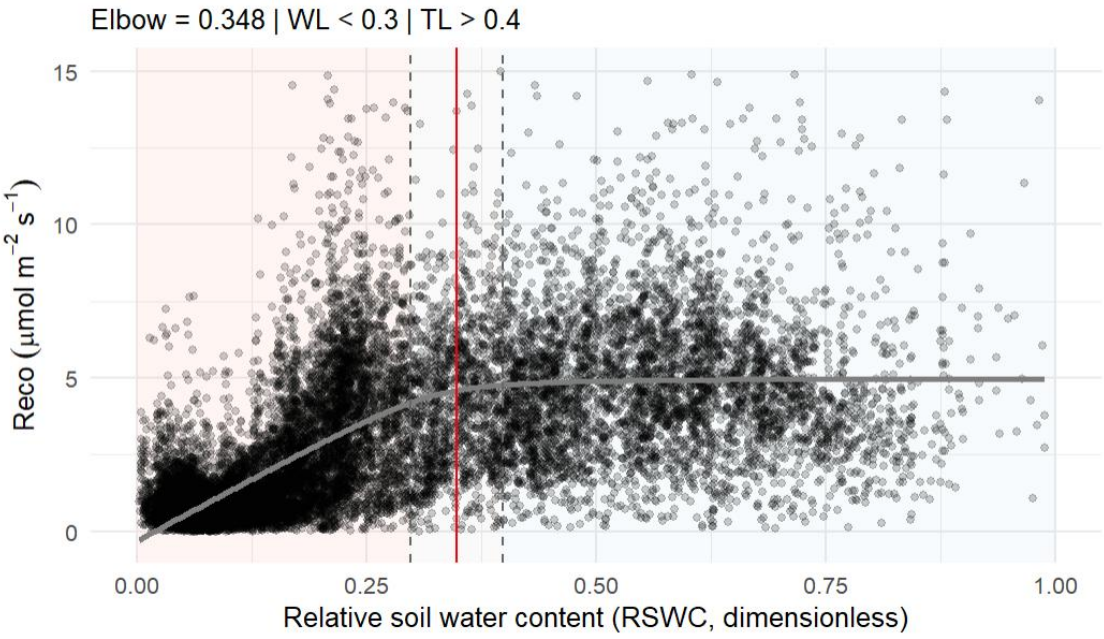

Figure 9: NRH fit of Reco against RSWC. The red line indicates the moisture threshold separating water-limited (WL) and temperature-limited (TL) regimes.

Composite analyses of five-day windows around birch events showed that fluxes peaked within 24h of rain when antecedent soil moisture was low (< 25th percentile RSWC) and temperature moderate (60 – 100th percentile) (Fig. 10).

Under these conditions, fluxes reached 5–8 µmol CO_2 m^{-2} s^{-1}. In contrast, responses were weak when antecedent soils were moist, with little effect of temperatures. These patterns indicate a coupled moisture–temperature optimum, with the strongest Birch-pulses occurring with soil desiccation, consistent with the NRH-derived regime structure.

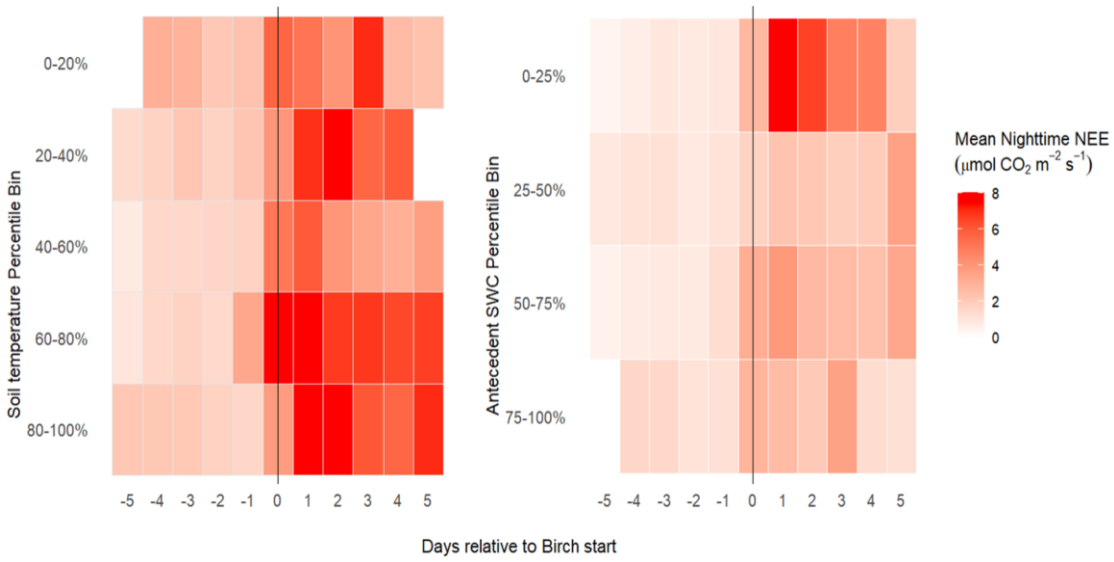

Figure 10: Heatmaps showing mean nighttime NEE across a) soil temperature and b) antecedent soil moisture percentile bins relative to Birch onset.

3.2. Moisture Correction Evaluation

Including soil moisture markedly improved model prediction under non-pulse conditions. The temperature-only model systematically underestimated fluxes during moderately dry periods, whereas the moisture-augmented model increased explained variance by ~25% and reduced random error by one-third (Table 1).

Table 1: Performance metrics for baseline Reco models.

	R^2	**RMSE**	**MAE**	**Bias**
R_{temp}	0.43	1.72	1.29	−0.17
$R_{moisture}$	0.72	1.22	0.82	−0.08

These improvements confirm that Reco depends on non-linear interactions between soil temperature and moisture rather than temperature alone.

3.3. BIRCH-PULSE MODEL EVALUATION

Model performance was evaluated during birch events (Table 2):

Table 2: Performance metrics for Birch event Reco models.

	R^2	RMSE	MAE	Bias
R_{temp}	−0.20	4.83	2.40	−1.71
$R_{moisture}$	−0.06	4.53	2.15	−1.93
R_{PT}	0.70	2.40	0.90	−0.15

Both R_{temp} and $R_{moisture}$ performed poorly during Birch events, yielding negative R^2 values and large residual errors. In contrast, the R_{PT} formulation achieved $R^2 = 0.70$ and reduced bias by an order of magnitude, confirming that explicitly representing a peak-and-decay dynamic captures the short-lived Reco surges missed by models designed for non-pulse, steady state conditions and therefore, Birch-pulse bias correction is necessary to capture the full magnitude of Reco.

3.4. CUMULATIVE AND TEMPORAL VALIDATION

Model evaluation across the full timeseries confirmed that explicitly representing pulse–decay dynamics improves carbon-budget closure (Table 3).

Table 3: Integrated performance of metrics for Reco models across entire timeseries

	Total Predicted Carbon (g C m^{-2})	Bias (µmol CO_2 m^{-2} s^{-1})	Bias (g C m^{-2})	Percent Bias (%)	Capture Ratio	RMSE (µmol CO_2 m^{-2} s^{-1})	NSE
R_{temp}	385.99	-2.52×10^6	−30.23	−7.26 %	0.93	2.06	0.34
$R_{moisture}$	397.84	-1.53×10^6	−18.38	−4.42 %	0.96	1.63	0.58
R_{PT}	401.50	-1.23×10^6	−14.72	−3.54 %	0.96	1.56	0.62

All models sufficiently reproduced total Reco within ±7 % of observations with $R_{moisture}$ and R_{PT} showing increasing prediction accuracy respectively. DTW diagnostics corroborated these findings by confirming their temporal realism (Table 4).

Table 4: Reco models dynamic performance metrics.

	Weighted DTW (↓)	NSE (SST-weighted) (↑)	Spearman ϱ (↑)	Cosine Similarity (↑)
R_{temp}	1.02	−0.50	−0.13	0.54
$R_{moisture}$	0.74	−0.24	0.24	0.64
R_{PT}	0.61	0.24	0.62	0.80

R_{PT} outperformed both baseline formulations across all similarity metrics, showing superior alignment in the timing and shape of Reco trajectories. The R_{PT} formulation performed best, followed by $R_{moisture}$ and R_{temp}, indicating that explicitly modelling pulse–decay dynamics within a moisture-orientated context improves both temporal fidelity and overall carbon-budget closure of Birch events amongst typical ecosystem functioning.

Event-integrated comparisons further showed that R_{PT} matched observed cumulative carbon release the closest, whereas baseline formulations lagged during the 12 hours following rainfall, exhibiting gross divergence (Fig. 11a). Cumulative absolute-error trajectories confirmed the least deviation for R_{PT} from observations across all events (Fig. 11b).

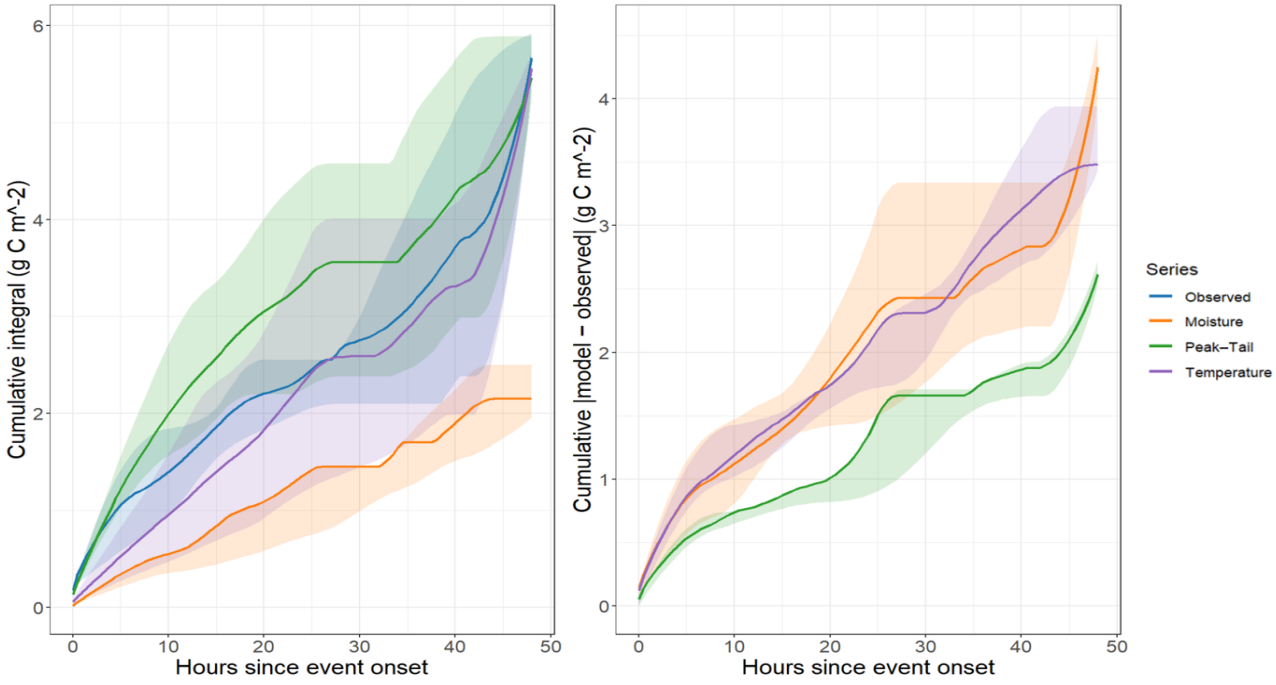

Figure 11: Event-aggregated cumulative respiration and model deviation.
a) Cumulative carbon emission (mean ± IQR) post rainfall events indicates that R_{temp} most closely matches observed totals.
b) Cumulative absolute deviation reveals that, despite this apparent agreement, R_{temp} ultimately diverges, while R_{PT} maintains the lowest overall error.

Collectively, these validations demonstrate that incorporating an explicit peak–decay structure yields consistent improvements in predictive skill, dynamic fidelity, and carbon-budget accuracy across the entire observation period.

3.5. XML Elucidation of Non-linear Pulse Drivers

XGBoost effectively captured Reco dynamics during Birch-pulse events, predicting observed flux variability with high accuracy on independent confirming that the selected predictors captured nearly all Reco variability (Table 5).

Table 5. Performance metrics of the R_{XGB}

	R^2	**RMSE**	**MAE**	**Bias**
R_{XGB}	0.979	0.218	0.138	0.034

Feature-importance analysis showed that Reco variability during Birch-pulses was chiefly governed by hydrological history and event timing (Fig. 12). ΔSWC Dryspan, Wet Pos, and ΔSWC 24h dominated model variance, while steady-state moisture, temperature, and meteorological variables exerted secondary influence, indicating control by antecedent drying and phase progression metrics rather than instantaneous meteorological conditions.

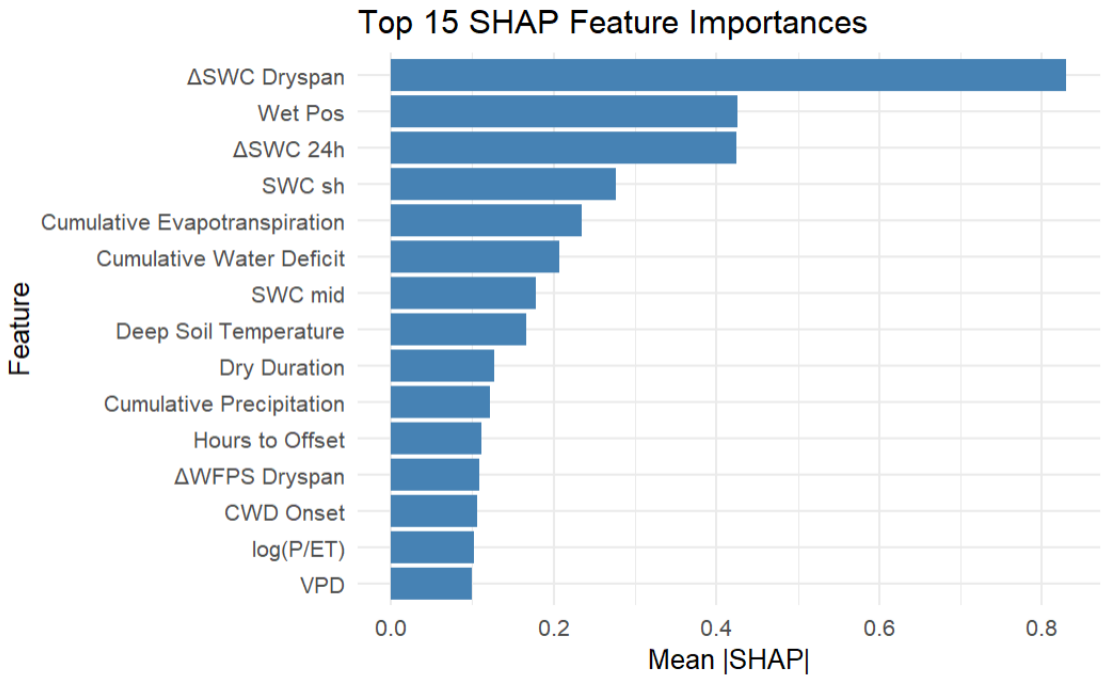

Figure 12: Top 15 predictors ranked by mean absolute SHAP value from the XGBoost model

SHAP dependence plots revealed distinct non-linear effects across key predictors (Fig. 13). Prediction of Reco increased with rewetting intensity (ΔSWC 24h) and wet-phase progression (Wet Pos), while antecedent drying (ΔSWC Dryspan) showed a sharp positive effect beyond a threshold, consistent with microbial reactivation after prolonged desiccation. SWC sh exhibited saturation at high moisture, and Cumulative ET and CWD displayed opposing influences linked to evaporative demand and drought stress.

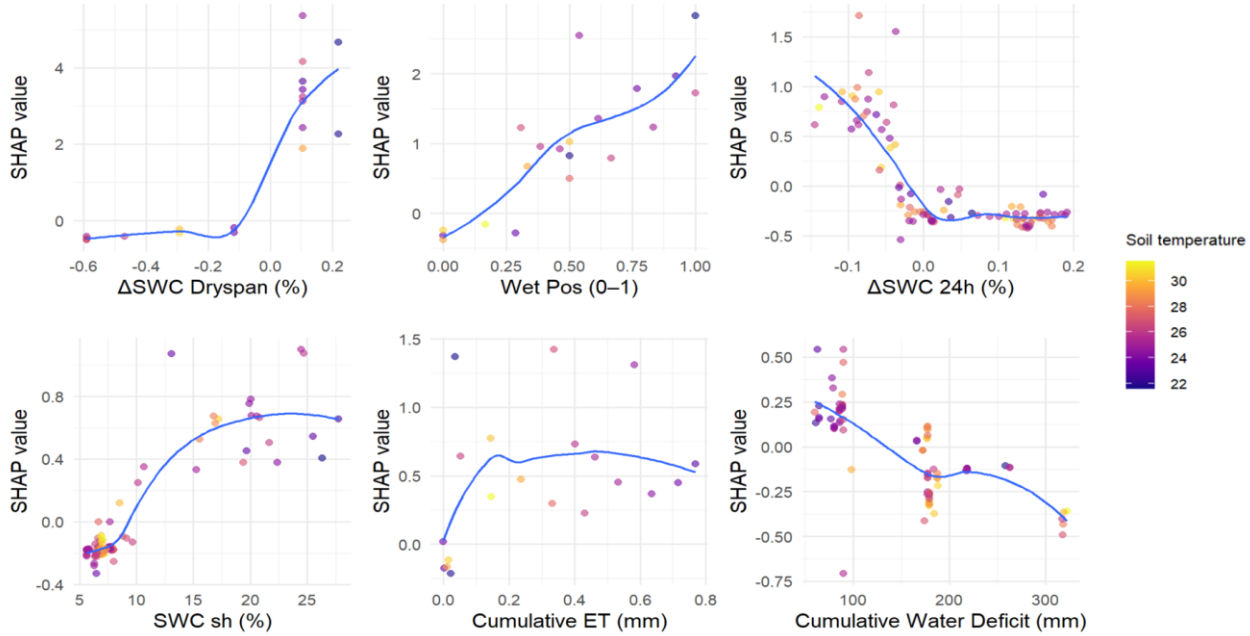

Figure 13: SHAP dependence plots showing marginal effects of key Reco predictors during Birch-pulse periods.

Thermal colour gradients indicated that high soil temperatures under dry or water-deficit conditions were associated with weak or negative SHAP values, highlighting suppression of fluxes under combined thermal and hydric stress. Collectively, Reco predictions were most responsive to antecedent drying and rewetting dynamics, with smaller contributions from temperature and evaporative demand.

4. DISCUSSION

4.1. MOISTURE CONTROLS ON RECO

The magnitude of observed Reco ($Reco_{obs}$) displayed a clear dependence on increasing soil moisture, from dry to moderately moist conditions before plateauing beyond a threshold of RSWC =0.348 (Fig. 9). Below this threshold, soil moisture and Reco remain closely coupled, highlighting the importance of moisture in relieving metabolic inhibition during soil desiccation. Beyond it, each incremental increase in RSWC yields a diminishing effect on Reco, implying that once soil structure and function are sufficiently reactivated, with substrate mobility stabilised and restored, additional wetting contributes little further stimulation. This inflection marks the transition from water-limited to temperature-limited regimes, consistent with established theory denoting the desiccation of microbial communities (Moyano *et al.*, 2012 ; Chang *et al.*, 2014). In theory, rewetting reactivates substrate diffusion, whereas excessive wetting may transiently suppress it through diffusion limitation or anoxia, conditions that rarely persist long enough in drylands to show a signal (Davidson & Janssens, 2006 ; Bond-Lamberty *et al.*, 2024).

Composite analyses of Birch-pulse periods (Fig. 10a) confirm that the largest CO_2 efflux occurred when dry antecedent soils were rewetted under moderately warm conditions. Although temperatures rarely fell below optimal, the highest Reco values coincided with

the warmest soils, where moderate heat promoted microbial activation and substrate turnover without exhibiting thermal inhibition (Xu *et al.*, 2004). Conversely, when antecedent soils were moist, post-rain Reco remained relatively unchanged, showing that both hydric and thermal constraints operate within distinct optimal ranges, but also relative to each other (Fig. 10b). In such cases, substrate diffusion, autotrophic respiration, and microbial resource competition are already near equilibrium, so additional wetting contributes little new metabolic stimulation. The rapid CO_2 surge and subsequent 24 hour decay typify the Birch effect, driven by osmotic shock and accelerated mineralization upon rewetting previously dry soils (Birch, 1958 ; Manzoni *et al.*, 2020 ; Meisner *et al.*, 2021). Similar patterns have been observed across Mediterranean, Sonoran, and Australian drylands, where pulse amplitude scales with the severity and duration of antecedent drought (Sponseller, 2007 ; Huxman *et al.*, 2004 ; Metz *et al.*, 2023).

Overall, these patterns support H1: Reco responses to rainfall pulses in semi-arid drylands are primarily governed by antecedent soil moisture, with temperature exerting only secondary influence, indicating that Birch-pulses arise from the interplay between abrupt soil rewetting and downstream thermal conditions.

4.2. MODELLING RECO UNDER MOISTURE CONSTRAINT

The comparison between the R_{temp} and $R_{moisture}$ formulations clearly demonstrates that Reco cannot be adequately represented by temperature-response functions alone. The inclusion of soil-moisture predictors substantially increased explanatory power and reduced model error relative to the temperature-only formulation (Table 1). The traditional R_{temp} model assumes continuous substrate availability and instantaneous microbial response, though arid soils experience strong moisture dependence through diffusion limitation of soluble substrates and microbial dormancy (Reichstein *et al.*, 2005 ; Vargas *et al.*, 2011 ; Moyano *et al.*, 2012). This improvement reflects the biophysical coupling between thermal and hydric states that govern microbial respiration.

However, both non-pulse formulations failed under birch conditions, with R_{temp} and $R_{moisture}$ producing negative coefficients of determination and large residual errors, consistent with similar contexts of model failure (Table 2) (Rousk & Brangarí, 2022). Both models consistently underestimated flux maxima, whereas R_{PT} closely matched both the amplitude and timing of observed responses (Fig. 11, 14). Across all events, Reco peaked within 12 hours of rainfall and then decayed exponentially, a pattern reproduced only by R_{PT}, markedly improving predictive skill and bias by an order of magnitude.

Evaluation across the entire time series showed that incorporating event segmentation improved both model accuracy and temporal fidelity (Table 3). R_{PT} achieved the highest NSE and lowest RMSE, reproducing cumulative C flux within ±3.54% of observations. DTW analyses indicated R_{PT} had the smallest shape distance and strongest phase alignment, confirming improved representation of event timing and magnitude (Table 4). These improvements reflect the model's ability to reproduce the delayed and asymmetric Birch dynamics governed by hydrological memory and post-rainfall decay, not merely an enhanced statistical fit. By explicitly parameterizing event-scale peak and decay dynamics, R_{PT} realistically captures the Birch effect trajectory and offers a process-informed yet parsimonious alternative to deterministic bias-correction frameworks (Nguyen *et al.*, 2025).

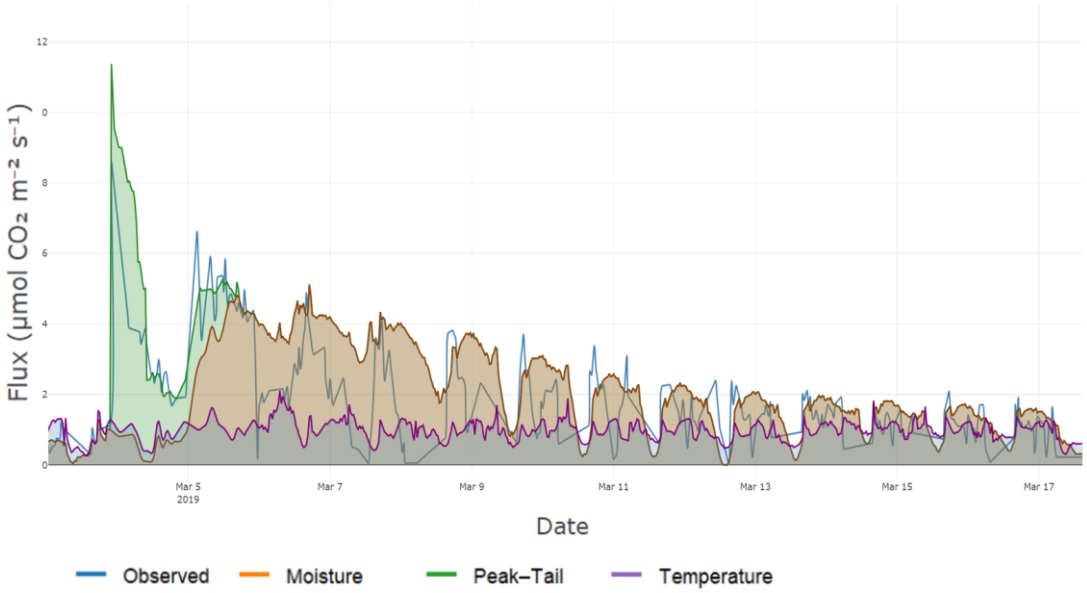

Figure 14: Time series of observed and modelled fluxes during a March 2019 Birch-pulse event, showing enhanced respiration following rewetting and improved fit of moisture- and event typology corrected models relative to the temperature-only baseline

Collectively, these results validate H2, showing that integrating soil-moisture context and event segmentation produces an empirical model that improves prediction while reflecting underlying ecohydrological controls. By resolving transient respiration dynamics rather than assuming steady-state temperature dependence, R_{PT} delivers bias-corrected flux estimates and a more mechanistic depiction of dryland processes. Its success underscores that temperature-based models must incorporate hydrological and temporal structure to capture the dominant sources of variability in semi-arid ecophysiology.

4.3. Non-Linear Interactions and Limitation Transitions

The XML feature importance analysis revealed that hydrological change-rate variables exerted the strongest influence on Birch-pulse Reco (Fig. 12). ΔSWC Dryspan and ΔSWC 24h ranked highest in SHAP feature importance, followed by Wet Pos and SWC sh.

SHAP dependence patterns for ΔSWC Dryspan, ΔSWC 24h, and CWD (Fig. 13a, c, f) highlight the dominant role of antecedent hydrology in shaping respiration pulses. Each variable captures a different facet of hydrological memory: the cumulative desiccation preceding rainfall (ΔSWC Dryspan), the immediate pre-event moisture change rate (ΔSWC 24 h), and the longer-term climatic water deficit (CWD). A clear breakpoint near ΔSWC ≈ 0 indicates that only true desiccation, not minor moisture gains, primes soils for Birch-type responses.

The positive SHAP response to increasing ΔSWC Dryspan indicates that stronger antecedent desiccation enhances R_{XGB}, while the linear decline in SHAP values for ΔSWC24 h toward zero shows that R_{XGB} predictions are best when the rate of change right before the wet onset are greatest. Together, these patterns highlight that Reco sensitivity is driven by the intensity of prior desiccation rather than the wetting phase itself, an outcome consistent with literature on the effects of drought-induced substrate accumulation and the persistence of stress-tolerant microbial communities (Moyano *et al.*, 2013 ; Borken & Matzner, 2009).

Within-event dynamics represented by Wet Pos and SWC sh (Fig. 13b, d) reveal how Reco evolves through the wet phase following rewetting. SHAP values for Wet Pos increased nearly linearly, indicating progressive microbial activation and substrate turnover as moisture persisted. In contrast, SWC sh showed a monotonic saturating relationship, where each incremental rise in soil water yielded a diminishing effect on predicting Reco, reflecting declining marginal moisture sensitivity as soils approached optimal wetness. A cluster of high-temperature, low-SWC points with negative SHAP values further illustrates that elevated temperature alone did not enhance flux under moisture limitation. Together, these patterns mark the complex transition of feature importance through time within Birch-pulses.

The weakly structured, multimodal pattern of Cumulative ET, together with the temperature gradients across predictors, indicates that evaporative demand and thermal energy impose complex secondary controls on respiration (Fig. 13e). Moderate evapotranspiration likely promotes gas diffusion and oxygen exchange, briefly enhancing CO_2 efflux, whereas sustained or intense evaporative demand depletes surface moisture and suppresses microbial activity. The overlaid thermal gradients show that respiration sensitivity declines sharply under concurrent warmth and dryness, demonstrating that high temperature amplifies physiological stress rather than stimulating flux when water is limiting. These results highlight an interactive constraint between water and energy availability, where moisture dynamics govern activation and temperature modulates the rate and persistence of post-rewetting respiration.

Collectively, the XML analysis demonstrates that respiration during Birch-pulse periods is governed by transient, rather than steady-state, hydrological conditions. Dependence plots show that Reco sensitivity is strongest to rate-based variables (ΔSWC Dryspan, ΔSWC 24 h), indicating that phase changes across the dry–wet boundary, rather than absolute environmental states, drive Birch magnitude and variability. The consistent sequence, antecedent drying followed by rapid rewetting and moderated by evaporative and thermal feedbacks, reflects the complex non-linear dynamic transition of environmental interactions, well documented in the literature. These patterns underscore that Birch-pulses emerge from non-equilibrium hydrological transitions.

Together, these results support H3, showing that Reco variability during pulse events is primarily governed by non-linear dry–wet transitions rather than absolute soil moisture, with temperature amplifying Reco only once critical moisture variables reach their respective optima and timing. These result aligns with recent machine-learning applications that utilised a knowledge-guided deep-learning model explicitly encoding rewetting cycles and diel hysteresis to successfully reproduce Reco pulses in semi-arid soils (Jiang *et al.*, 2022).

5. CONCLUSION

5.1. SYNTHESIS

This thesis investigated the drivers and modelling of Reco responses to rainfall pulses in a semi-arid East African dryland context, addressing how antecedent conditions, event characteristics, and temporal dynamics shape carbon flux variability. Across event-scale, empirical modelling, and machine-learning analyses, the results converge on a central conclusion: Reco is primarily controlled by hydrological dynamics and temporally structured by dry–wet transitions when soil moisture is limited. From a modelling perspective, incorporating soil-moisture context and event segmentation markedly improved the capacity of statistical predictions to reproduce observed flux variability, while explainable ensemble models provided complementary insight into the complex, non-linear interactions underlying these responses. The findings demonstrate that Reco variability in drylands cannot be reproduced by temperature functions alone, and undeniably require hydrologically contextualised models that utilise event segmentation, such as the R_{PT} or FluxPulse, to yield bias-corrected, event-preserving accurate estimates of Reco (Nguyen *et al.*, 2025). Together, these insights strengthen the conceptual basis for representing pulse-driven Reco dynamics in water-limited ecosystems.

5.2. LIMITATIONS AND FUTURE DIRECTIONS

Initially, a core theme of this study was intended to compare the performance of contrasting model paradigms that are contemporarily defining flux research: empirically grounded, data-driven approaches such as the developed R_{PT}, and geometrically constrained, decay-fitting frameworks such as FluxPulse (Nguyen *et al.*, 2025). Beyond assessing performance, the goal was to contribute to the wider debate between empirical models that extract patterns directly from observations and parameterised models that impose predefined biological functions (Tang *et al.*, 2024). In practice, however, the comparison was limited by the structural design of FluxPulse. Although it provides a robust interannual-to-annual, multi-site bias-correction framework, its architecture is hard-coded to detect Birch-pulses lasting at least 48 hours. At Kapiti, most respiration pulses were ephemeral bursts triggered by brief rainfall events, after which the system quickly reverted to moisture limitation, ultimately being too transient for which FluxPulse was conceived. Originally designed for interannual multi-site bias corrections, the model's architecture, while powerful for long-duration pulses, proved ill-suited to the short, transient Birch responses characteristic of the Kapiti savanna.

Several ecophysiological factors introduced limitation to this study. Firstly, a key issue is the reliance on nighttime fluxes for model calibration. This assumes that respiration–temperature relationships derived under nocturnal conditions also hold during the day, yet diel decoupling of soil temperature frequently violates this assumption. Because daytime soils are typically warmer and more thermally variable, models constrained to nighttime data likely underestimate total respiration and overlook the stronger temperature sensitivity and moisture–temperature interactions expressed under daytime conditions (Han *et al.*, 2023). The focus on a single semi-arid savanna site further restricts generalisation across drylands, where differences in soil texture, rooting depth, and vegetation traits strongly influence pulse responses. Additional uncertainty arises from preferential flow paths: in highly desiccated soils, rewetting proceeds unevenly as rainfall infiltrates through large exposed fissures, producing spatially heterogeneous wetting

fronts (Pushpanjali *et al.*, 2025 ; Ribeiro Filho *et al.*, 2023). This induces two biases: (i) vertical heterogeneity in soil moisture redistribution, as preferential infiltration bypasses surface layers, and (ii) spatial heterogeneity in CO_2 efflux, as these fissures temporarily act as conduits for subsurface gas release (DeCarlo & Caylor, 2020). Such non-uniform rewetting and effluxes violate the assumption of homogeneous flux surfaces implicit in EC measurements, likely contributing to sub-grid noise in the flux signature and variability not captured by the models.

From a methodological perspective, several structural and technical limitations should be noted. The IRGA suffers intermittent data loss when raindrops accumulate on the optical bench, ironically during periods most critical for pulse analysis (Heusinkveld *et al.*, 2008). Such interference can truncate flux records and bias model calibration, though rigorous despiking, flag screening, and cross-sensor validation were applied to minimise these artefacts. The event-typology framework introduces an additional source of subjectivity, as fixed thresholds inevitably simplify the continuum of ecohydrological states in which overlapping wet–dry sequences are common. Although these thresholds were empirically derived from multi-year data and validated against soil-moisture responses, they cannot fully reproduce the gradient nature of pulse dynamics. Model structure and parsimony also present challenges. Complex algorithms such as XGBoost risk overfitting site-specific patterns, whereas simplified GAM-based models may omit key interactions. Belowground processes, including root exudation, priming, and non-diffusive gas transport, remain unrepresented but were partially accounted for by focusing on relative, event-scale variability to isolate ecohydrological signals from unmodelled biological noise (Vereecken *et al.*, 2016).

Future research should extend the framework to coupled Reco–GPP models, enabling a more comprehensive assessment of savanna ecophysiological dynamics and the timing and magnitude of growing-period sink responses relative to the associated Birch-pulse (Feldman *et al.*, 2024). Chamber campaigns offering multiple replicates (bare soil, vegetation present, field capacity, wilting point) would enable a more comprehensive Reco model by partitioning autotrophic and heterotrophic contributions under varied moisture conditions (Tang & Baldocchi, 2005). Regional upscaling could be achieved by calibrating event-scale models with CHIRPS rainfall, MODIS LST, and Sentinel-2 NDVI/EVI, linking flux-tower observations to spatial patterns of rainfall-pulse prediction, post-wetting responses, and carbon-cycle dynamics across East African drylands (Palmer *et al.*, 2023 ; Lucht, 2011). Comparative sensitivity analyses between the R_{PT} and FluxPulse formulations across contrasting dryland sites are essential to evaluate parameter robustness and model transferability (Jian *et al.*, 2024). Such analyses would clarify whether differences in predicted Reco arise from parameter values or structural assumptions, thereby identifying which components of each framework are generalisable versus site-specific.

5.3. Ecological and Climatic Significance

The role of antecedent soil moisture and dry-period duration in this study underscores the significance of ecohydrology in regulating carbon exchange in East Africa. As precipitation regimes become increasingly intense and episodic, the frequency and magnitude of respiration pulses are likely to increase, potentially offsetting productivity gains and weakening the regions carbon-sink capacity (Ahlström et al., 2015; Nguyen et al., 2025). Notably, intensification of rain events may also extend soil-moisture persistence, sustaining microbial and root activity for longer durations. The overall carbon balance could therefore have a greater dependency on the interplay between microbial

activation, substrate availability, and diffusive limitation, an uncertainty that long-term flux networks are well positioned to constrain (Hao *et al.*, 2025). These findings highlight the need to treat drylands not as uniformly carbon-limited systems but as ecosystems whose function emerges from short-lived, precipitation-driven flux events.

5.4. Applied Relevance and Outlook

Beyond advancing methodology, this study offers operational value for improving regional Reco partitioning, carbon accounting and ecophysiological monitoring in East Africa (Dinku *et al.*, 2014). The event-based approach and the R_{PT} framework can be integrated into flux-network bias-correction workflows, helping to interpret abrupt Reco pulses in critically arid dryland landscapes that are too brief for existing models to explain. This framework has the potential to underpin spatially explicit productivity forecasts across East African drylands, informing sustainable rangeland management and climate-adaptation strategies, aligning with ILRI's goals to translate ecosystem-scale science into actionable, data-driven tools for land-use and climate mitigation (Boone *et al.*, 2018).

5.5. Closing Synthesis

Collectively, this work demonstrates that understanding the event-scale mechanisms governing dryland productivity is essential to predicting how semi-arid ecosystems will respond to intensifying rainfall variability. By uniting empirical and data-driven perspectives, this thesis provides a foundation for scaling semi-arid pulse-driven processes within regional flux networks and global biogeochemical models. Overall, the findings demonstrate that in dryland ecophysiology, the sensitivity of productivity is inscribed not in the slow progression of seasons, but in the complex cadence of rainfall pulses.

6. REFERENCES

Abram N.J., Gagan M.K., Cole J.E., Hantoro W.S., & Mudelsee M. 2008. Recent intensification of tropical climate variability in the Indian Ocean. *Nature Geoscience*, 1(12), p. 849-853. DOI : 10.1038/ngeo357

Ago E.E., Agbossou E.K., Cohard J.-M., Galle S., & Aubinet M. 2016. Response of CO2 fluxes and productivity to water availability in two contrasting ecosystems in northern Benin (West Africa). *Annals of Forest Science*, 73(2), p. 483-500.

Ai J., Qi X., Zhang R., He M., Li J., Xu R., Li Y., Sarmah S., Wang H., & Zhao J. 2023. A novel approach for ecosystem respiration simulation in drylands. *Frontiers in Ecology and Evolution*, 11. Available at : https://www.frontiersin.org/journals/ecology-and-evolution/articles/10.3389/fevo.2023.1186272/full (Accessed1 novembre 2025).

Anadón J.D., Sala O.E., & Maestre F.T. 2014. Climate change will increase savannas at the expense of forests and treeless vegetation in tropical and subtropical Americas. *Journal of Ecology*, 102(6), p. 1363-1373. DOI : 10.1111/1365-2745.12325

Aubinet M., Vesala T., & Papale D. 2012. *Eddy covariance: a practical guide to measurement and data analysis*. Springer Science & Business Media

Barnes M.L., Farella M.M., Scott R.L., Moore D.J., Ponce-Campos G.E., Biederman J.A., MacBean N., Litvak M.E., & Breshears D.D. 2021. Improved dryland carbon flux predictions with explicit consideration of water-carbon coupling. *Communications Earth & Environment*, 2(1), p. 248.

Beven K. & Germann P. 1982. Macropores and water flow in soils. *Water Resources Research*, 18(5), p. 1311-1325. DOI : 10.1029/WR018i005p01311

Bieri M., Du Toit J., Maluta N.E., Mantlana B., Mateyisi M., Midgley G.F., Mutanga S., von Maltitz G., & Brummer C. 2022. Integrating project-based infrastructures with long-term greenhouse gas observations in Africa. *Clean Air Journal*, 32(1), p. 1-9.

Birch H. 1958. The effect of soil drying on humus decomposition and nitrogen availability. *Plant and soil*, 10, p. 9-31.

Bliefernicht J., Berger S., Salack S., Samuel G., Hingerl L., Heinzeller D., Mauder M., Steinbrecher R., Steup G., Bossa A.Y., Waongo M., Quansah E., Balogun A., Yacouba Y., Arnault J., Wagner S., Klein C., Gessner U., Knauer K., & Kunstmann H. 2018. The WASCAL Hydrometeorological Observatory in the Sudan Savanna of Burkina Faso and Ghana. *Vadose Zone Journal*, 17. DOI : 10.2136/vzj2018.03.0065

Bond-Lamberty B., Ballantyne A., Berryman E., Fluet-Chouinard E., Jian J., Morris K.A., Rey A., & Vargas R. 2024. Twenty years of progress, challenges, and opportunities in measuring and understanding soil respiration. *Journal of Geophysical Research: Biogeosciences*, 129(2), p. e2023JG007637.

Boone R.B., Conant R.T., Sircely J., Thornton P.K., & Herrero M. 2018. Climate change impacts on selected global rangeland ecosystem services. *Global change biology*, 24(3), p. 1382-1393.

Borken W. & Matzner E. 2009. Reappraisal of drying and wetting effects on C and N mineralization and fluxes in soils. *Global change biology*, 15(4), p. 808-824.

Burba G.G., Mcdermitt D.K., Grelle A., Anderson D.J., & Xu L. 2008. Addressing the influence of instrument surface heat exchange on the measurements of CO2 flux from open-path gas analyzers. *Global Change Biology*, 14(8), p. 1854-1876.

Canarini A., Kaiser C., Merchant A., Richter A., & Wanek W. 2019. Root Exudation of Primary Metabolites: Mechanisms and Their Roles in Plant Responses to Environmental Stimuli. *Frontiers in Plant Science*, 10. Available at : https://www.frontiersin.org/journals/plant-science/articles/10.3389/fpls.2019.00157/full (Accessed27 mai 2025).

Chang C.-T., Sabaté S., Sperlich D., Poblador S., Sabater F., & Gracia C. 2014. Does soil moisture overrule temperature dependence of soil respiration in Mediterranean riparian forests? *Biogeosciences*, 11(21), p. 6173-6185.

Chen S., Lin G., Huang J., & Jenerette D. 2009. Dependence of carbon sequestration on the differential responses of ecosystem photosynthesis and respiration to rain pulses in a semiarid steppe. *Global Change Biology*, 15, p. 2450-2461. DOI : 10.1111/j.1365-2486.2009.01879.x

Chen T. & Guestrin C. 2016. Xgboost: A scalable tree boosting system. Dans : *Proceedings of the 22nd acm sigkdd international conference on knowledge discovery and data mining*. p. 785-794.

Collins S.L., Sinsabaugh R.L., Crenshaw C., Green L., Porras-Alfaro A., Stursova M., & Zeglin L.H. 2008. Pulse dynamics and microbial processes in aridland ecosystems. *Journal of Ecology*, 96(3), p. 413-420.

Dannenberg M.P., Barnes M.L., Smith W.K., Johnston M.R., Meerdink S.K., Wang X., Scott R.L., & Biederman J.A. 2023. Upscaling dryland carbon and water fluxes with artificial neural networks of optical, thermal, and microwave satellite remote sensing. *Biogeosciences*, 20(2), p. 383-404. DOI : 10.5194/bg-20-383-2023

Davidson E.A. & Janssens I.A. 2006. Temperature sensitivity of soil carbon decomposition and feedbacks to climate change. *Nature*, 440(7081), p. 165-173.

DeCarlo K.F. & Caylor K.K. 2020. Effects of crack morphology on soil carbon flux dynamics in a dryland vertisol. *Geoderma*, 375, p. 114478.

Dinku T., Block P., Sharoff J., Hailemariam K., Osgood D., del Corral J., Cousin R., & Thomson M.C. 2014. Bridging critical gaps in climate services and applications in Africa. *Earth Perspectives*, 1(1), p. 15.

Donat M.G., Lowry A.L., Alexander L.V., O'Gorman P.A., & Maher N. 2016. More extreme precipitation in the world's dry and wet regions. *Nature Climate Change*, 6(5), p. 508-513.

Douville H., Raghavan K., Renwick J., Allan R.P., Arias P.A., Barlow M., Cerezo-Mota R., Cherchi A., Gan T., & Gergis J. 2021. Water cycle changes.

Emmerich W.E. 2003. Carbon dioxide fluxes in a semiarid environment with high carbonate soils. *Agricultural and Forest Meteorology*, 116(1), p. 91-102. DOI : 10.1016/S0168-1923(02)00231-9

Feldman A.F., Feng X., Felton A.J., Konings A.G., Knapp A.K., Biederman J.A., & Poulter B. 2024. Plant responses to changing rainfall frequency and intensity. *Nature Reviews Earth & Environment*, 5(4), p. 276-294.

Fischer E.M., Beyerle U., & Knutti R. 2013. Robust spatially aggregated projections of climate extremes. *Nature Climate Change*, 3(12), p. 1033-1038.

Foken T., Aubinet M., & Leuning R. 2011. The eddy covariance method. Dans : *Eddy covariance: A practical guide to measurement and data analysis*. Springer, p. 1-19.

Friedman J. 2009. The elements of statistical learning: Data mining, inference, and prediction. *Springer*, (2nd edition).

Frouz J. & Bujalský L. 2018. Flow of CO2 from soil may not correspond with CO2 concentration in soil. *Scientific Reports*, 8(1), p. 10099.

Galvin K., Boone R., Smith N., & Lynn S. 2001. Impacts of climate variability on East African pastoralists: linking social science and remote sensing. *Climate Research*, 19, p. 161-172. DOI : 10.3354/cr019161

Galvin K.A. 2009. Transitions: Pastoralists Living with Change. *Annual Review of Anthropology*, 38(1), p. 185-198. DOI : 10.1146/annurev-anthro-091908-164442

Goodfellow I. 2016. *Deep learning*. MIT press

Haile G.G., Tang Q., Hosseini-Moghari S.-M., Liu X., Gebremicael T.G., Leng G., Kebede A., Xu X., & Yun X. 2020. Projected Impacts of Climate Change on Drought Patterns Over East Africa. *Earth's Future*, 8(7), p. e2020EF001502. DOI : 10.1029/2020EF001502

Han Y., Wang G., Zhou S., Li W., & Xiong L. 2023. Day–night discrepancy in soil respiration varies with seasons in a temperate forest. *Functional Ecology*, 37(7), p. 2002-2013.

Hao Y., Mao J., Bachmann C.M., Hoffman F.M., Koren G., Chen H., Tian H., Liu J., Tao J., & Tang J. 2025. Soil moisture controls over carbon sequestration and greenhouse gas emissions: a review. *npj climate and atmospheric science*, 8(1), p. 16.

Heusinkveld B.G., Jacobs A.F.G., & Holtslag A.A.M. 2008. Effect of open-path gas analyzer wetness on eddy covariance flux measurements: A proposed solution. *Agricultural and Forest Meteorology*, 148(10), p. 1563-1573. DOI : 10.1016/j.agrformet.2008.05.010

Huxman T.E., Snyder K.A., Tissue D., Leffler A.J., Ogle K., Pockman W.T., Sandquist D.R., Potts D.L., & Schwinning S. 2004. Precipitation pulses and carbon fluxes in semiarid and arid ecosystems. *Oecologia*, 141, p. 254-268.

IPCC I.P.O.C. 2007. *Climate Change 2007: The Physical Science Basis. Contribution of Working Group I to the Fourth Assessment Report of the Intergovernmental Panel on Climate Change*. Cambridge, United Kingdom and New York, NY, USA : Cambridge University Press, 996 p.

James G., Witten D., Hastie T., & Tibshirani R. 2013. *An introduction to statistical learning: with applications in R*. Springer

Jarvis P., Rey A., Petsikos C., Wingate L., Rayment M., Pereira J., Banza J., David J., Miglietta F., & Borghetti M. 2007. Drying and wetting of Mediterranean soils stimulates decomposition and carbon dioxide emission: the « Birch effect ». *Tree physiology*, 27(7), p. 929-940.

Jenerette G.D., Scott R.L., & Huxman T.E. 2008. Whole ecosystem metabolic pulses following precipitation events. *Functional Ecology*, 22(5), p. 924-930.

Jian S., Li J., Wang G., Zhou J., Schadt C.W., & Mayes M.A. 2024. Generalizing microbial parameters in soil biogeochemical models: Insights from a multi-site incubation experiment. *Journal of Geophysical Research: Biogeosciences*, 129(4), p. e2023JG007825.

Jiang P., Chen X., Missik J.E., Gao Z., Liu H., & Verbeke B.A. 2022. Encoding diel hysteresis and the Birch effect in dryland soil respiration models through knowledge-guided deep learning. *Frontiers in Environmental Science*, 10, p. 1035540.

Jiang Z., Bian H., Xu L., Li M., & He N. 2021. Pulse Effect of Precipitation: Spatial Patterns and Mechanisms of Soil Carbon Emissions. *Frontiers in Ecology and Evolution*, 9. Available at : https://www.frontiersin.org/journals/ecology-and-evolution/articles/10.3389/fevo.2021.673310/full (Accessed27 mai 2025).

Jung M., Reichstein M., & Bondeau A. 2009. Towards global empirical upscaling of FLUXNET eddy covariance observations: validation of a model tree ensemble approach using a biosphere model. *Biogeosciences*, 6(10), p. 2001-2013.

Kaimal J.C. & Finnigan J.J. 1994. *Atmospheric boundary layer flows: their structure and measurement*. Oxford university press

Kew S.F., Philip S.Y., Hauser M., Hobbins M., Wanders N., Van Oldenborgh G.J., Van Der Wiel K., Veldkamp T.I., Kimutai J., & Funk C. 2021. Impact of precipitation and increasing temperatures on drought trends in eastern Africa. *Earth System Dynamics*, 12(1), p. 17-35.

Kieft T.L., soroker E., & firestone M.K. 1987. Microbial biomass response to a rapid increase in water potential when dry soil is wetted. *Soil Biology and Biochemistry*, 19(2), p. 119-126. DOI : 10.1016/0038-0717(87)90070-8

Knapp Alan K., Beier C., Briske D.D., Classen A.T., Luo Y., Reichstein M., Smith M.D., Smith S.D., Bell J.E., & Fay P.A. 2008. Consequences of more extreme precipitation regimes for terrestrial ecosystems. *Bioscience*, 58(9), p. 811-821.

Knapp Alan K, Beier C., Briske D.D., Classen A.T., Luo Y., Reichstein M., Smith M.D., Smith S.D., Bell J.E., & Fay P.A. 2008. Consequences of more extreme precipitation regimes for terrestrial ecosystems. *Bioscience*, 58(9), p. 811-821.

Lado-Monserrat L., Lull C., Bautista I., Lidón A., & Herrera R. 2014. Soil moisture increment as a controlling variable of the « Birch effect ». Interactions with the pre-wetting soil moisture and litter addition. *Plant and Soil*, 379(1), p. 21-34. DOI : 10.1007/s11104-014-2037-5

Liang G., Reed S.C., Stark J.M., & Waring B.G. 2023. Unraveling mechanisms underlying effects of wetting–drying cycles on soil respiration in a dryland. *Biogeochemistry*, 166(1), p. 23-37.

Lindh M., Zhang L., Falster D., Franklin O., & Brännström Å. 2014. Plant diversity and drought: The role of deep roots. *Ecological modelling*, 290, p. 85-93.

Lucht W. 2011. *A Continental–Scale Estimate of Ecosystem Respiration Using MODIS Land Surface Temperature and Enhanced Vegetation Index*. NASA Ames Research Center

Lundberg S.M., Erion G., Chen H., DeGrave A., Prutkin J.M., Nair B., Katz R., Himmelfarb J., Bansal N., & Lee S.-I. 2020. From local explanations to global understanding with explainable AI for trees. *Nature machine intelligence*, 2(1), p. 56-67.

Manzoni S., Chakrawal A., Fischer T., Schimel J.P., Porporato A., & Vico G. 2020. Rainfall intensification increases the contribution of rewetting pulses to soil heterotrophic respiration. *Biogeosciences*, 17(15), p. 4007-4023. DOI : 10.5194/bg-17-4007-2020

Manzoni S., Schimel J.P., & Porporato A. 2012. Responses of soil microbial communities to water stress: results from a meta-analysis. *Ecology*, 93(4), p. 930-938.

McMillen R.T. 1988. An eddy correlation technique with extended applicability to non-simple terrain. *Boundary-Layer Meteorology*, 43(3), p. 231-245. DOI : 10.1007/BF00128405

Meisner A., Snoek B.L., Nesme J., Dent E., Jacquiod S., Classen A.T., & Priemé A. 2021. Soil microbial legacies differ following drying-rewetting and freezing-thawing cycles. *The ISME Journal*, 15(4), p. 1207-1221.

Metz E.-M., Vardag S.N., Basu S., Jung M., Ahrens B., El-Madany T., Sitch S., Arora V.K., Briggs P.R., & Friedlingstein P. 2023. Soil respiration–driven CO2 pulses dominate Australia's flux variability. *Science*, 379(6639), p. 1332-1335.

Meyer N., Welp G., & Amelung W. 2018. The Temperature Sensitivity (Q10) of Soil Respiration: Controlling Factors and Spatial Prediction at Regional Scale Based on Environmental Soil Classes. *Global Biogeochemical Cycles*, 32(2), p. 306-323.

Moncrieff J.B., Massheder J.M., de Bruin H., Elbers J., Friborg T., Heusinkveld B., Kabat P., Scott S., Soegaard H., & Verhoef A. 1997. A system to measure surface fluxes of momentum, sensible heat, water vapour and carbon dioxide. *Journal of Hydrology*, 188-189, p. 589-611. DOI : 10.1016/S0022-1694(96)03194-0

Moyano F.E., Manzoni S., & Chenu C. 2013. Responses of soil heterotrophic respiration to moisture availability: An exploration of processes and models. *Soil Biology and Biochemistry*, 59, p. 72-85. DOI : 10.1016/j.soilbio.2013.01.002

Moyano F.E., Vasilyeva N., Bouckaert L., Cook F., Craine J., Curiel Yuste J., Don A., Epron D., Formanek P., & Franzluebbers A. 2012. The moisture response of soil heterotrophic respiration: interaction with soil properties. *Biogeosciences*, 9(3), p. 1173-1182.

Muthoka J.M., Rowhani P., Salakpi E., Balzter H., & Antonarakis A. 2025. Classification of grassland community types and palatable pastures in semi-arid savannah grasslands of Kenya using multispectral Sentinel-2 imagery. *Frontiers in Sustainable Food Systems*, 9, p. 1543491.

Ndlovu E., Prinsloo B., & Le Roux T. 2020. Impact of climate change and variability on traditional farming systems: Farmers' perceptions from south-west, semi-arid Zimbabwe. *Jàmbá: Journal of Disaster Risk Studies*, 12(1), p. 1-19.

Nguyen N.B., Migliavacca M., Bassiouni M., Baldocchi D.D., Gherardi L.A., Green J.K., Papale D., Reichstein M., Cohrs K.-H., Cescatti A., Nguyen T.D., Nguyen H.H., Nguyen Q.M., & Keenan T.F. 2025. Widespread underestimation of rain-induced soil carbon emissions from global drylands. *Nature Geoscience*, 18(9), p. 869-876. DOI : 10.1038/s41561-025-01754-9

Niang I., Ruppel O., Abdrabo M., Essel A., Lennard C., Padgham J., & Urquhart P. 2017. Climate change 2014: impacts, adaptation, and vulnerability. Part B: regional aspects. *Contribution of Working Group II to the Fifth Assessment Report of the Intergovernmental Panel on Climate Change*, , p. 1199-1265.

Nicholson S.E. 2018. The ITCZ and the Seasonal Cycle over Equatorial Africa. Available at : https://journals.ametsoc.org/view/journals/bams/99/2/bams-d-16-0287.1.xml (Accessed10 février 2025).

Odongo V.O., Leitner S., Räsänen M., Omondi J.O., Pellikka P., Vesala T., Heiskanen J., Rinne J., Dowling T.P.F., & Korczynski J. 2025. Environmental controls on peak carbon uptake across four Kenyan dryland ecosystems.

Palmer P.I., Wainwright C.M., Dong B., Maidment R.I., Wheeler K.G., Gedney N., Hickman J.E., Madani N., Folwell S.S., Abdo G., Allan R.P., Black E.C.L., Feng L., Gudoshava M., Haines K., Huntingford C., Kilavi M., Lunt M.F., Shaaban A., & Turner A.G. 2023. Drivers and impacts of Eastern African rainfall variability. *Nature Reviews Earth & Environment*, 4(4), p. 254-270. DOI : 10.1038/s43017-023-00397-x

Pastorello G., Trotta C., Canfora E., Chu H., Christianson D., Cheah Y.-W., Poindexter C., Chen J., Elbashandy A., & Humphrey M. 2020. The FLUXNET2015 dataset and the ONEFlux processing pipeline for eddy covariance data. *Scientific data*, 7(1), p. 225.

Placella S.A., Brodie E.L., & Firestone M.K. 2012. Rainfall-induced carbon dioxide pulses result from sequential resuscitation of phylogenetically clustered microbial groups. *Proceedings of the National Academy of Sciences*, 109(27), p. 10931-10936.

Pushpanjali, Reddy K.S., Dhimate A.S., Karthikeyan K., Samuel J., Reddy A.G.K., Ravi Kumar N., Rao K.V., Pankaj P.K., & Rohit J. 2025. Soil preferential flow dynamics in the southern drylands of India—a watershed based approach. *Frontiers in Water*, 6, p. 1457680.

Rabbi S.M., Warren C.R., Swarbrick B., Minasny B., McBratney A.B., & Young I.M. 2024. Microbial decomposition of organic matter and wetting–drying promotes aggregation in artificial soil but porosity increases only in wet-dry condition. *Geoderma*, 447, p. 116924.

Reichstein M. 2005. On the separation of net ecosystem exchange into assimilation and ecosystem respiration: review and improved algorithm. *Global change biology*, 11(9), p. 1424-1439.

Reichstein M., Falge E., Baldocchi D., Papale D., Aubinet M., Berbigier P., Buchmann N., Gilmanov T., Granier A., Grünwald T., Havránková K., Ilvesniemi H., Janous D., Knohl A., Laurila T., Lohila A., Loustau D., & Matteucci G. 2005. On the Separation of Net Ecosystem Exchange into Assimilation and Ecosystem Respiration: Review and Improved Algorithm. *Global Change Biology*, 11, p. 1424-1439. DOI : 10.1111/j.1365-2486.2005.001002.x

Ribeiro Filho J.C., Andrade E.M. de, Guerreiro M.S., Palácio H.A. de Q., & Brasil J.B. 2023. Soil–Water–Atmosphere Effects on Soil Crack Characteristics under Field Conditions in a Semiarid Climate. *Hydrology*, 10(4), p. 83.

Rousk J. & Brangarí A.C. 2022. Do the respiration pulses induced by drying–rewetting matter for the soil–atmosphere carbon balance? *Global Change Biology*, 28(11), p. 3486.

Rudin C. 2019. Stop explaining black box machine learning models for high stakes decisions and use interpretable models instead. *Nature machine intelligence*, 1(5), p. 206-215.

Sala O.E. & Lauenroth W.K. 1982. Small rainfall events: An ecological role in semiarid regions. *Oecologia*, 53(3), p. 301-304. DOI : 10.1007/BF00389004

Sánchez-García C., Oliveira B.R.F., Keizer J.J., Doerr S.H., & Urbanek E. 2020. Water repellency reduces soil CO2 efflux upon rewetting. *Science of The Total Environment*, 708, p. 135014. DOI : 10.1016/j.scitotenv.2019.135014

SCF S.C.F. 2025. *SCD0003: Module for Eddy Covariance-Based Continuous Quantification of Greenhouse Gas Fluxes* (1.0). Resilient Planet, Sustainable Livelihoods : Social Carbon Foundation, Available at : https://www.socialcarbon.org/ (Accessed26 octobre 2025).

Schimel J., Balser T.C., & Wallenstein M. 2007. Microbial stress-response physiology and its implications for ecosystem function. *Ecology*, 88(6), p. 1386-1394.

Schimel J.P. 2018. Life in Dry Soils: Effects of Drought on Soil Microbial Communities and Processes. *Annual Review of Ecology, Evolution, and Systematics*, 49(Volume 49, 2018), p. 409-432. DOI : 10.1146/annurev-ecolsys-110617-062614

Schwinning S. & Sala O.E. 2004. Hierarchy of responses to resource pulses in arid and semi-arid ecosystems. *Oecologia*, 141(2), p. 211-220. DOI : 10.1007/s00442-004-1520-8

Seghieri J. 1995. The rooting patterns of woody and herbaceous plants in a savanna; are they complementary or in competition? *African Journal of Ecology*, 33(4), p. 358-365.

Senegal I., Namibia O., Abdrabo M., Ama E., Lennard C., (USA J., Africa P., Adelekan I., Archibald S., (Cameroon M., Barkhordarian A., Battersby J., (USA E., (USA M., (Tunisia M., (USA/India M., Chineke T., (Netherlands K., Houria D., & Leary N. 2014. Chapter 22 Africa. In: Climate Change 2014: Impacts, Adaptation, and Vulnerability. Part B: Regional Aspects. Contribution of Working Group II to the Fifth Assessment Report of the Intergovernmental Panel on Climate Change. , p. 1199-1265.

Shukla P.R., Skeg J., Buendia E.C., Masson-Delmotte V., Pörtner H.-O., Roberts D.C., Zhai P., Slade R., Connors S., & Van Diemen S. 2019. Climate Change and Land: an IPCC special report on climate change, desertification, land degradation, sustainable land management, food security, and greenhouse gas fluxes in terrestrial ecosystems.

Singh S., Mayes M.A., Kivlin S.N., & Jagadamma S. 2023. How the Birch effect differs in mechanisms and magnitudes due to soil texture. *Soil Biology and Biochemistry*, 179, p. 108973.

Sponseller R.A. 2007. Precipitation pulses and soil CO2 flux in a Sonoran Desert ecosystem. *Global Change Biology*, 13(2), p. 426-436.

Stoy P.C., Chu H., Dahl E., Cala D.S., Shveytser V., Wiesner S., Desai A.R., & Novick K.A. 2023. The global distribution of paired eddy covariance towers. *bioRxiv*, , p. 2023.03.03.530958.

Tang J. & Baldocchi D.D. 2005. Spatial–temporal variation in soil respiration in an oak–grass savanna ecosystem in California and its partitioning into autotrophic and heterotrophic components. *Biogeochemistry*, 73(1), p. 183-207.

Tang J., Riley W.J., Manzoni S., & Maggi F. 2024. Feasibility of formulating ecosystem biogeochemical models from established physical rules. *Journal of Geophysical Research: Biogeosciences*, 129(6), p. e2023JG007674.

Unks R.R., Goldman M.J., Mialhe F., Gunnell Y., & Hemingway C. 2023. Diffuse land control, shifting pastoralist institutions, and processes of accumulation in southern Kenya. *The Journal of Peasant Studies*, 50(5), p. 1757-1790.

Vardag S.N., Metz E.-M., Artelt L., Basu S., & Butz A. 2025. CO2 release during soil rewetting shapes the seasonal carbon dynamics in South American Temperate region. *Geophysical Research Letters*, 52(8), p. e2024GL111725.

Vargas R., Carbone M.S., Reichstein M., & Baldocchi D.D. 2011. Frontiers and challenges in soil respiration research: from measurements to model-data integration. *Biogeochemistry*, 102(1), p. 1-13.

Vereecken H., Schnepf A., Hopmans J.W., Javaux M., Or D., Roose T., Vanderborght J., Young M.H., Amelung W., & Aitkenhead M. 2016. Modeling soil processes: Review, key challenges, and new perspectives. *Vadose zone journal*, 15(5), p. vzj2015. 09.0131.

Vickers D. & Mahrt L. 1997. Quality Control and Flux Sampling Problems for Tower and Aircraft Data. *Journal of Atmospheric and Oceanic Technology*, 14(3), p. 512-526. DOI : 10.1175/1520-0426(1997)014%3C0512:QCAFSP%3E2.0.CO;2

Wang B., Zha T.S., Jia X., Wu B., Zhang Y.Q., & Qin S.G. 2014. Soil moisture modifies the response of soil respiration to temperature in a desert shrub ecosystem. *Biogeosciences*, 11(2), p. 259-268. DOI : 10.5194/bg-11-259-2014

Warren C.R. 2014. Response of osmolytes in soil to drying and rewetting. *Soil Biology and Biochemistry*, 70, p. 22-32.

Webb E.K., Pearman G.I., & Leuning R. 1980. Correction of flux measurements for density effects due to heat and water vapour transfer. *Quarterly Journal of the Royal Meteorological Society*, 106(447), p. 85-100. DOI : 10.1002/qj.49710644707

Wieckowski A., Vestin P., Ardö J., Roupsard O., Ndiaye O., Diatta O., Ba S., Agbohessou Y., Fensholt R., & Verbruggen W. 2024. Eddy covariance measurements reveal a decreased carbon sequestration strength 2010–2022 in an African semiarid savanna. *Global Change Biology*, 30(9), p. e17509.

Wood J.M., Bremer E., Csonka L.N., Kraemer R., Poolman B., van der Heide T., & Smith L.T. 2001. Osmosensing and osmoregulatory compatible solute accumulation by bacteria. *Comparative Biochemistry and Physiology Part A: Molecular & Integrative Physiology*, 130(3), p. 437-460. DOI : 10.1016/S1095-6433(01)00442-1

Xu L., Baldocchi D.D., & Tang J. 2004. How soil moisture, rain pulses, and growth alter the response of ecosystem respiration to temperature. *Global Biogeochemical Cycles*, 18(4).

7. LIST OF ABBREVIATIONS

EC:	Eddy Covariance
NEE:	Net Ecosystem Exchange
Reco:	Ecosystem Respiration
GPP:	Gross Primary Productivity
SWC:	Soil Water Content
RSWC:	Relative Soil Water Content
WFPS:	Water-Filled Pore Space
CWD:	Climatic Water Deficit
PPFD:	Photosynthetic Photon Flux Density
R_{temp}:	Reco Temperature-Response Curve Model
$R_{moisture}$:	Reco Moisture Corrected
R_{PT}:	Reco Peak - Tail
R_{XGB}:	Reco XGBoost
DTW:	Dynamic Time Warping
NSE:	Nash–Sutcliffe Efficiency
RMSE:	Root Mean Square Error
MAE:	Mean Absolute Error
QC:	Quality Control
SHAP:	Shapley Additive Explanations
GAM:	Generalised Additive Model
XGBoost:	Extreme Gradient Boosting
IRGA:	Infrared Gas Analyser
ITCZ:	Intertropical Convergence Zone
IOD:	Indian Ocean Dipole
ENSO:	El Niño–Southern Oscillation
CHIRPS:	Climate Hazards Group InfraRed Precipitation with Station data
MODIS:	Moderate Resolution Imaging Spectroradiometer

8. TABLE OF TABLES

9. TABLE OF FIGURES

10. APPENDICES

TABLE OF APPENDICES

APPENDIX 1: INSTRUMENTATION AND MEASUREMENT SPECIFICATIONS

Table A1. Instruments deployed at Kapiti, their manufacturers, measured variables, heights, and sampling frequencies.

Measurement category	Instrument	Manufacturer	Measured variables	Height	Sampling
Eddy-Covariance System	WindMaster Pro 3D sonic anemometer	Gill Instruments Ltd (UK)	3D wind velocity (u,v,w), sonic temperature (T_s)	4.3 m	10 Hz (LI-COR SmartFlux)
	LI-7500DS open-path Infrared Gas Analyser (IRGA)	LI-COR Biosciences (USA)	CO_2, H_2O densities (μmol mol^{-1})	4.3 m	10 Hz (synchronised with anemometer)
	SmartFlux System + CR1000X datalogger	LI-COR / Campbell Scientific (USA)	Data acquisition & synchronisation	Tower base	Continuous
Biometeorological sensors	HMP155 probes (2)	Vaisala Oyj (Finland)	Air temperature, relative humidity	2–4 m	1 Hz → 30-min means
	TR-525M tipping-bucket gauge	LI-COR Biosciences (USA)	Precipitation	1.5 m	1 tip = 0.2 mm
	CNR4 net radiometer	Kipp & Zonen (Netherlands)	Net radiation (SW in/out, LW in/out)	4 m	1 Hz → 30-min means
	LI-190R quantum sensor	LI-COR Biosciences (USA)	Photosynthetic photon flux density (PPFD, 400–700 nm)	4 m	1 Hz → 30-min means
Soil microclimate sensors	ECH_2O 5TM sensors (3)	METER Group (USA)	Volumetric soil water content (θ)	5, 15, 30 cm depth	1 Hz → 30-min means
	107 thermistors (3)	Campbell Scientific (USA)	Soil temperature (T_s)	5, 15, 30 cm depth	1 Hz → 30-min means
Ancillary systems	Solar-battery array + controller	Campbell Scientific (USA)	12 V power supply	—	—
	Sutron 9210 datalogger	Sutron Corp (USA)	Redundant T, RH, radiation, rainfall archive	2–4 m	1 Hz → 30-min means
Flux computation & corrections	EddyPro v7.0 software	LI-COR Biosciences (USA)	CO_2, H_2O, H, LE, τ fluxes + diagnostics	—	Post-processing (30 min)

APPENDIX 2: DATA PROCESSING WORKFLOW

High-frequency raw data were processed in EddyPro v7.0 following FLUXNET Tier 1 protocols (Pastorello *et al.*, 2020). Key steps included:

1. **Coordinate rotation:** to align the vertical axis with the mean flow ($\bar{w} = 0$) (McMillen, 1988).
2. **Time-lag correction:** by covariance maximisation (±1 s) between wind and scalar signals (Foken *et al.*, 2011).
3. **Plausibility filtering:** removing physically impossible values |NEE| > 50 μmol CO_2 m^{-2} s^{-1} (Vickers & Mahrt, 1997).
4. **Spectral transfer corrections** for high- and low-frequency attenuation (Moncrieff *et al.*, 1997).
5. **Density correction (WPL)** converting raw covariances to true molar fluxes of CO_2 and H_2O (Webb *et al.*, 1980).

Quality-controlled 30-min flux data were processed in R (v4.5.2) and merged with biometeorology records. Data gaps ≤3h were linearly interpolated, and fluxes with QC >1 were excluded. All time series were converted to UTC +3 and integrated into a unified multiyear dataset (2018–2020) indexed by date-time.

APPENDIX 3: ENVIRONMENTAL COVARIATES

Table A3. Derived environmental covariates metrics used in the analysis, including their descriptions, equations, and units.

Variable group	Description	Equation	Unit
Soil moisture normalisation	Relative soil water content (RSWC): Normalised to field capacity and wilting point to express plant-available water fraction.	$\frac{\theta - \theta_{wp}}{\theta_{fc} - \theta_{wp}}$	(0–1)
	Water-filled pore space (WFPS): Proportion of total soil porosity occupied by water.	$\frac{\theta}{1 - \frac{\rho_b}{\rho_p}}$	fraction
Soil moisture and thermal metrics	Difference change in shallow soil moisture over x-h interval (ΔSWC_{6h}, ΔSWC_{24h})	$\theta_t - \theta_{t-\tau}$	$m^3\ m^{-3}\ h^{-1}$
	Cumulative rate of desiccation during preceding dry period (ΔSWC_dryspan)	$\frac{\theta_{onset} - \theta_{start}}{t_{onset} - t_{start}}$	$m^3\ m^{-3}\ h^{-1}$
	Total precipitation accumulated within each wet event (P_wet_total)	$\sum_{t \in wet} P_t$	mm
	Running cumulative precipitation and evapotranspiration since wet onset (CumP_t, CumET_t)	$\sum_{i=t_{onset}}^{t} P_i \text{ or } ET_i$	mm
Hydrological balance metrics	Ratio of cumulative precipitation to evapotranspiration during wet period (P/ET_since_wet)	$\frac{CumPt}{CumETt}^{since\ wet\ onset}$	–
	Log-transformed wet-phase P/ET ratio (log(P/ET))	$log(\frac{P + \alpha}{ET + \alpha})$	–
	Running climatic water deficit (CWD_running): Cumulative Evaporative Stress	$_{max}(0, CWD_{t-1} + (ET_t - P_t))$	mm
	Antecedent Cumulative Water Deficit (ET – P) at Birch onset	$\sum_{i \in dry} (ET_i - P_i)$	mm
Temporal descriptors	Elapsed time since wet-period onset (hrs_since_wet_onset)	$t - t_{wet\ onset}$	h
	Elapsed time since preceding dry-period onset (hrs_since_dry_onset)	$t - t_{dry\ onset}$	h
	Total length of wet or associated dry period (Wet_duration_hr, Dry_duration_hr)	$t_{onset} - t_{offset}$	h
	Normalised position within wet window (Wet_Pos)	$\frac{t - t_{wet\ onset}}{t_{wet\ offset} - t_{wet\ onset}}$	0 = onset 1 = offset)

Symbol	Description
θ	Volumetric soil-water content ($m^3\ m^{-3}$)
wp	Observed wilting point
fc	Observed field capacity
ρ_b	Bulk density (1.3 g cm^{-3})
ρ_p	Particle density (2.65 g cm^{-3})
t	Time (h)
τ	Differencing interval (h)
α	Stabilising constant (0.1 mm)